Chapter 6
Estimating crown projected area from remote sensing at different spatial resolution and its use in estimating DBH

6.1 Introduction

Previously, Chapter 2 highlighted the potential of crown projected area to infer DBH of the scattered Eucalyptus trees. Chapter 5 subsequently explores the use of tree shadows to infer tree height. With the array of very high resolution datasets now available, the question is 'how well can multispectral images of different spatial resolution estimate crown projection area?' This chapter investigates two different datasets from different remote sensing systems; one of 15 cm (airborne), and the other of 50 cm (airborne and spaceborne) spatial resolution for estimating the crown projection area of scattered eucalypt species.

Large Scale Photographs (LSP) and photomensuration methods have largely replaced on-ground methods of estimating planimetric crown area, or more correctly 'crown projected area' (Bertolette and Spotskey, 1999; Clark et al., 2004). However, most of these approaches involved manual measurement on the derived data.

The choice of an appropriate scale, or spatial resolution, for a particular application depends on many factors which includes information desired about the ground scene, the analysis methods to be used to extract the information, and the spatial structure of the scene. Woodcock and Strahler (1987) carried out a study where they showed that the local variance of a digital image for a scene changed as the resolution-cell size changes. Their graphical process can help in selecting an appropriate image scale. These graphs could be obtained by imaging the scene at fine resolution and then sub-sampling (or block pixel-averaging) the image to successively coarser spatial resolution while calculating the local variance. Their findings confirmed that the local variance/resolution graphs for the forested, agricultural, and urban/suburban environments reveal the spatial structure of each type of scene, and that this is a function of the size and spatial relationships of the objects contained within the scene. At the spatial resolutions of SPOT and Thematic Mapper imagery, local image variance is relatively high for forested and urban/suburban environments, suggesting that information-extracting techniques utilizing texture, context, and mixture modeling are appropriate for these sensor systems. In agricultural environments, local variance is low, and the more traditional classifiers are appropriate.

Of course the spatial resolution of remotely sensed digital datasets can be as high as decimetres for both airborne (Chapter 2) and spaceborne (Chapter 3) sensors. Unlike Landsat or SPOT satellite data where a single pixels can encompass many tree crowns, or significant non-crown features, decimetre spatial resolution data makes crown assessment studies with single trees possible (e.g., Chapter 2 – Verma et al., 2014b, Chapter 3 – Verma et al., 2013; Palace et al., 2007; Song et al., 2010; Chopping, 2011). Chubey et al. (2006) modelled canopy cover directly based on spectral and spatial features of the image; on the other hand, Sanquetta et al. (2011) measured canopy area by projecting the canopy and then transferring to AutoCAD where the spatial location of each tree from the initial coordinate was adjusted to an adequate scale. Asner et al. (2002) used IKONOS data to map tree crown size and by comparing the results with ground measurements, they concluded that satellite based observations have overestimated larger crowns leaving the smaller crowns undetected. Song et al. (2010) studied the potential of using the behavior of image semivariograms at different spatial resolutions to estimate tree crown size from IKONOS and Quickbird images and concluded that this approach can provide estimates of average tree crown size for hardwood stands. They also concluded that the model can be generalized across sensors and sites. Greenberg et al. (2005) have effectively used IKONOS data (spatial resolution 4m) in estimating crown projected area, DBH and stem density. Even though high resolution remote sensing data have successfully been used in many applications, as discussed earlier, there are some challenges with a very high resolution data, including the increase of intra crown spectral variance and the low spectral separability between tree crowns and other vegetated surfaces in the understorey (Chapter 3 – Verma et al., 2014b; Gougeon and Leckie., 2006; Hirschmugl et al., 2007; Pouliot et al., 2002) limit the identification of tree crowns, particularly with pixel-based spectral classifiers. However, with introduction of contextual information into the classification process in the form of object based image analysis (OBIA) have bridged the gap between the increasing amount of detailed geospatial data and the inefficient results of conventional pixel based classifiers (Chapter 3 – Verma et al., 2014b; Blaschke, 2010). The details of OBIA were discussed earlier in Chapter 3 (Verma et al., 2014b).

Following Chapter 3 (Verma et al., 2014b), crown projected area can potentially be extracted from very high spatial resolution imagery by either of the two methods; manual or on screen digitization or by automated methods, for example segmentation and classification. Both of these methods will be tested in this chapter, and the compared with the field measurements of crown projected area. Furthermore, the allometric equation linking crown projected area with DBH developed earlier in Chapter 2 (Verma et al., 2014a) will also be applied and the performance of the two sensor datasets evaluated in terms of predicted DBH as compared to the on ground measured values.

6.2 Materials and Methods

6.2.1 Study Area

The study area was same as that used in Chapter 5, and is described in section 5.3.1.

6.2.2 Remote Sensing Datasets

The digital imagery used in this study was acquired from some sources already described in earlier chapters. Multispectral imagery of 15 cm spatial resolution was acquired using the Duncan Tech MS4100 camera system mounted in a Cessna 172 aircraft (described in Chapter 2, Verma et al, 2014b) and 50 cm multispectral imagery was acquired from the airborne ADS40 sensor (Section 5.4.2). A 50 cm spatial resolution, multispectral, PAN sharpened WorldView2 (WV2) orthoimage was also acquired on 1 January 2012 with four spectral bands (Blue 0.4-0.5 μm), Band 2 (Green 0.5-0.6 μm), Band 3 (Red 0.6-0.7 μm) and band 4 (NIR 0.7-1 μm). In order to compare the performance of the three datasets, only the three spectral bands common to all of the datasets, namely Green (0.5-0.6 μm), Red (0.6-0.7 μm) and NIR (0.7-1 μm) were used.

The two 50 cm spatial resolution images, namely the airborne ADS40 and spaceborne WV2 were resampled to 15 cm using nearest neighbor resampling technique to match with the resolution of MS4100 dataset for pixel wise comparison.

6.2.3 Field Data Collection

The same 172 individual mature Eucalypt trees used in the earlier allometric equation development (Chapter 2 – Verma et al., 2014a) was used in this study, and their presence in each of the three image datasets was confirmed. The characteristics of the trees are summarised in Table 2.2, Chapter 2.

The methods by which crown projected area (CA) and DBH were measured are also described in Section 2. 2.2 of Chapter 2.

6.3 Data Analysis

All three images were registered and georeferenced to WGS 84 UTM Zone 56 S projection systems.

6.3.1 Manual method (On screen vectorization)

On screen digitization of the tree crowns in the imagery involved manually vectorizing the tree crown envelope based on the visual interpretation. The process of vectorization was performed using the approach of Gougeon. (1995). This approach treats the brighter and darker pixels as tree crown and

shadow, respectively. The crown projected area was delineated from all the three image sets keeping the scale of the view constant during the vectorization process. This was to avoid any over and under estimations of the canopy area. Different sets of band combinations were tested to extract the tree crown projected area. Since tree crown are usually associated with shadows, hence to get a clear demarcation of shadows with trees both true colour composite (Red, Green and Blue Bands) and false colour composite (NIR, Red and Green) was tested. The true colour image gave the best interpretation results as it helped decipher the crown with shadowed areas. These results were based solely on the visual inspection. Onscreen digitization step similar to Ke and Quackenbush. (2010) was followed by the area calculation for each polygon representing tree crowns.

6.3.2 Automated method (Image Segmentation and Classification)

The second method of tree crown extraction involved segmentation of image features into objects and then classification of objects into a given class using a method called object based image analysis (OBIA). It is an automated approach which takes into account the form, textures and spectral information of the image, as discussed earlier in Chapter 3 (Verma et al., 2014b). The analysis was done in eCognition Developer 8 (Munich, Germany, GmbH; Blaschke and Strobl., 2001). Segmentation and classification was performed on all the three sensor datasets. The key 'adjustable' parameters in the segmentation process of scale, colour and shape have been discussed in Chapter 2. Again, the quality of the segmentation output was visually assessed for all the three images.

Following the segmentation process, a supervised nearest neighbour (NN) classification was used for the classification of the image objects. Since the prime objective of the study was to only extract the tree crowns, the images were classified into only two classes, namely 'tree' and 'no trees'. Features such as mean pixel value, brightness, standard deviation and area (number of pixels) were considered for the NN classification. Additional arithmetic features like the NDVI and the Ratio image (NIR and red) were also taken into account. However, no textural features, such as GLCM and GLDV contrasts were used as after a number of exploratory trial and error tests textural attribute did not appear to help in delineating the tree crowns. Following classification, the 'tree' class was exported as a separate shape file and then intersected with the sampling locations. The area of the tree crown polygons with information on sample number was recorded.

6.3.3 Statistical Analysis

The three sets of measured crown projected area were tested for normality (Q-Q plot and Shapiro Wilk test) and in case of non-normality, a transformation was carried out; this was assessed by performing the Wilcox test. Scatter plots were created based on the ground and remote sensing based

measurements using the statistical software R (Studio Version 0.97.318). The coefficient of determination (R^2) was used to evaluate the level of variance in the estimates.

The performance of each sensor was quantified using a mean prediction error (MPE) given by $MPE=\overline{|CA_{predicted}-CA_{actual}|}$ calculated.

6.4 Analysis Results

Examples of the classified tree polygons are given in Figure 6.1.

Although the spectral bands for each of the images were the same, the scale parameter which gave the best visual segmentation results varied among the three sets of images. The parameters shape and compactness remained the same for three images (shape = 0.7 and compactness = 0.5). The MS4100 image was segmented at a scale of 40 while ADS 40 and WV2 images were segmented at scale of 70 to get the optimum result.

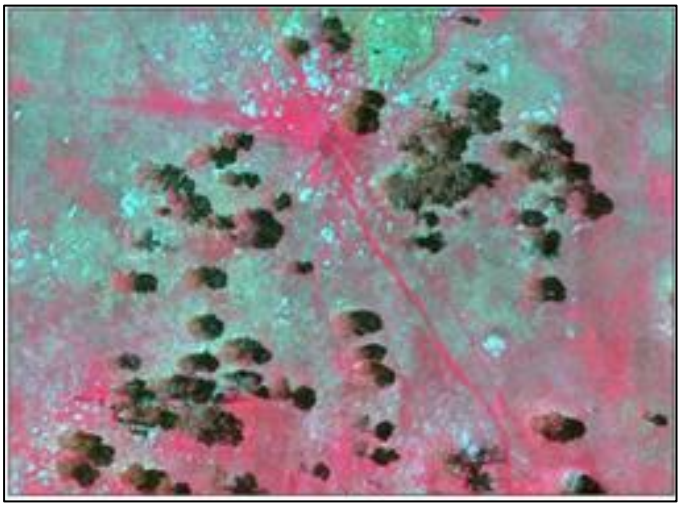

Color Infrared (CIR) image

(a) Tree extracted from CIR image

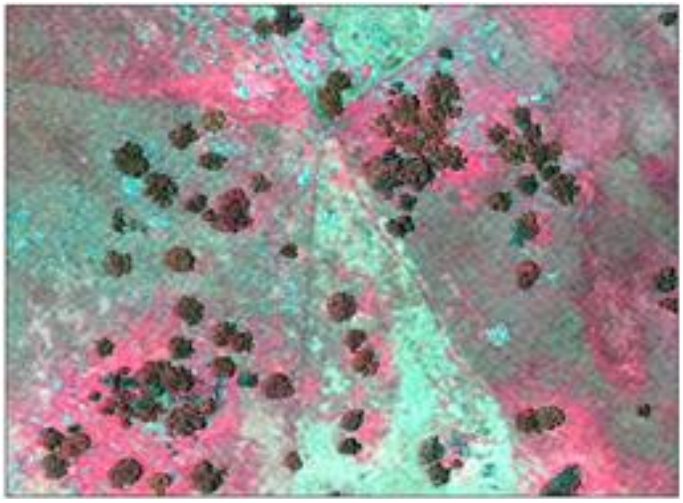

World View 2(WV2) image

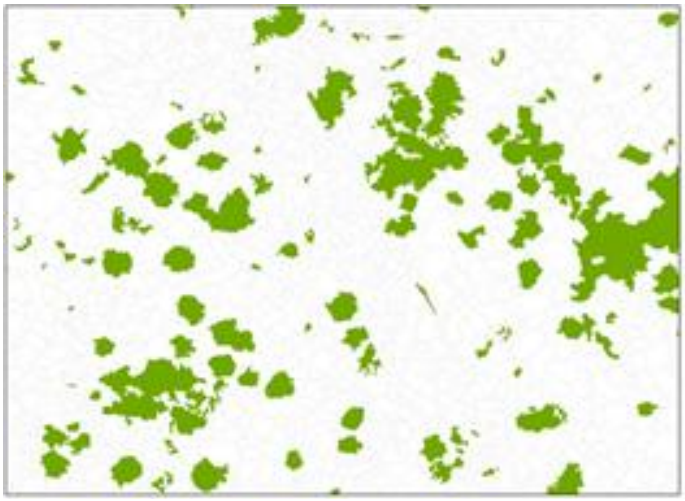

(b) Tree extracted from WV2 image

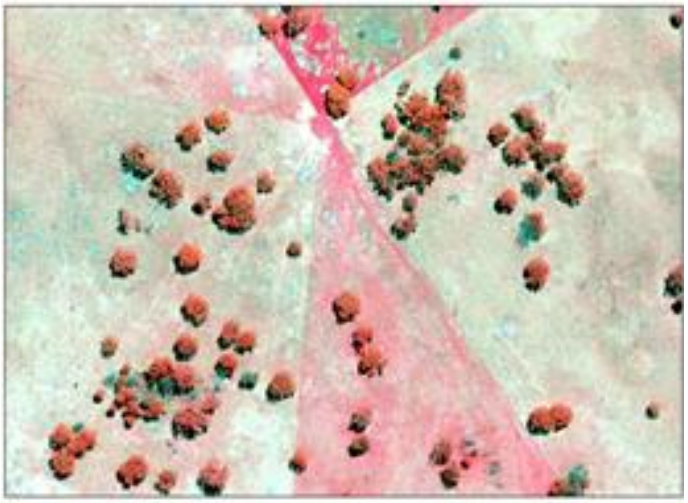

ADS40 image

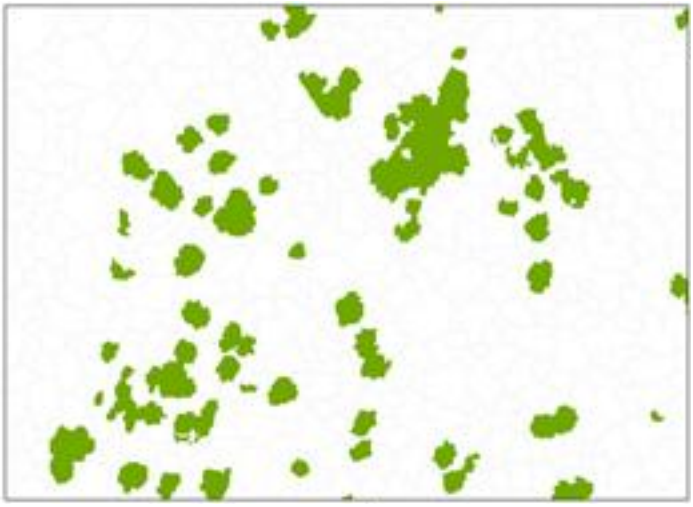

(c) Tree extracted from ADS40 image

Figure 6.1shows the trees generated by automated methods a) Color Infra red image b) World View2 image c) ADS 40 image

Figure 6.2 shows the scatter plots of field measured CA and manually delineated CA from different sensors. Regression analysis shows a good correlation between crown projected area estimates from manual method. Although the manual method of CA extraction was accurate WV2 and ADS 40 explained only ~70% of the variance in the CA (R^2 in the range of 0.67 to 0.68) with MPE of 55 and 53 m^2 respectively (26% and 25% respectively) whereas MS4100 showed a better performance by explaining 76% of variance with MPE of 48 m^2 (error of 22%). The CA measurement results from segmentation and classification shows similar trend. Figure 6.3 shows the scatter plots of field measured CA and automatically delineated CA from different sensors. As expected, error was higher in this case though not very significant. Interestingly WV2 results showed a decrease in MPE slightly (error down by 1%), whereas ADS40 and MS4100 showed an increased estimation error of 29% and 26% respectively compared to 25% and 22% by manual methods. Figure 6.4 shows the scatter plots of manual and segmentation based CA estimations in the three sensors. A very good agreement between crown projected area estimates from manual and automatic methods indicates that either of the two methods can be used with confidence.

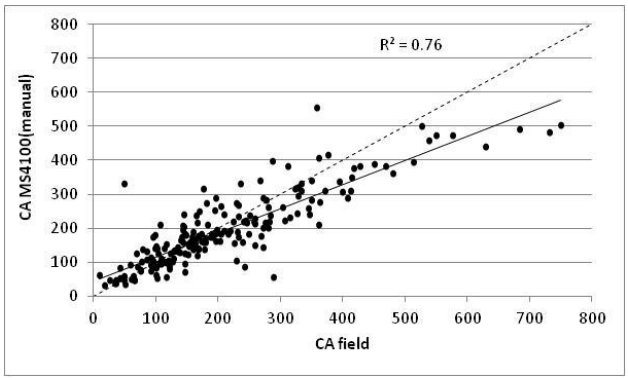

(a)

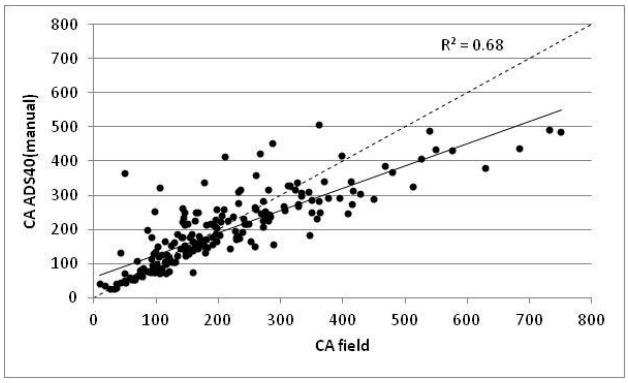

(b)

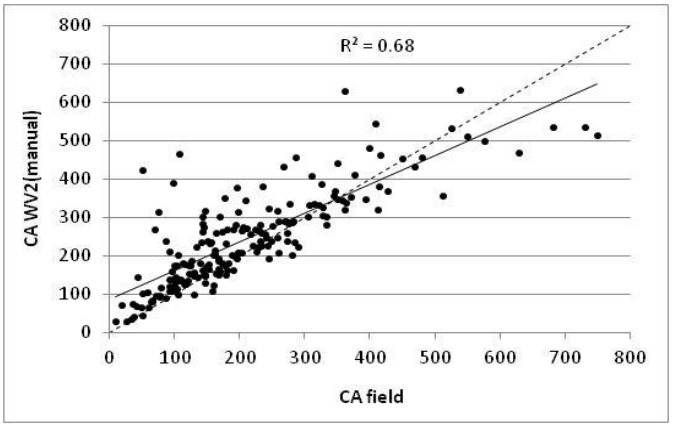

(c)

Figure 6.2. Scatter plots of the derived CA from each of the images versus the field-measured CA_{field}. (a) MS4100, (b) ADS40, and (c) WV2. The image-derived CA was calculated using manual vectorization; n = 172.

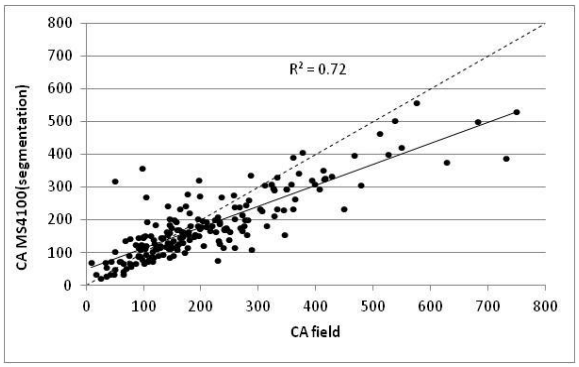

(a)

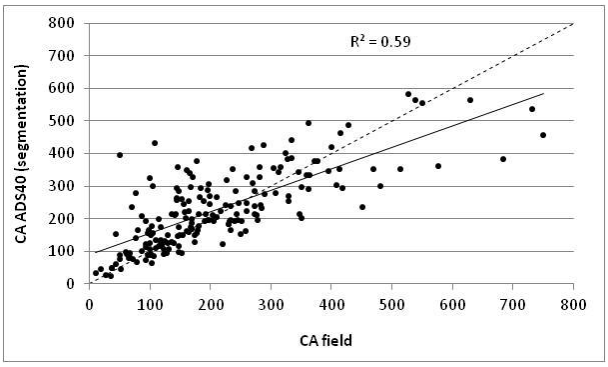

(b)

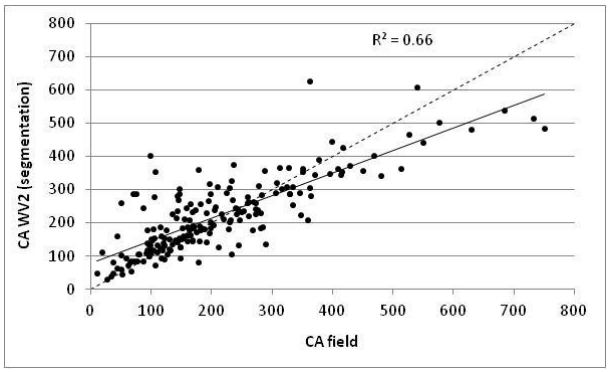

(c)

Figure 6.3. Scatter plots of the derived CA from each of the images versus the field-measured CA_{field}. (a) MS4100, (b) ADS40, and (c) WV2. The image-derived CA was calculated using image segmentation; n = 172.

A comparison of mean CA estimates by the three sensors using the two methods shows variations which appeared to be non-significant. As against the observed mean field based measurement value (211), MS4100 image showed a mean value of 183 (underestimation), ADS40 -229 and WV2 a mean of 221. The mean CA values for both segmentation and manual methods were almost comparable except for WV2 where the manual method of extraction resulted in overestimation of the CA. For MS4100, as compared to the manual method, segmentation method showed underestimation of canopies, whereas ADS40 showed overestimation of canopies but not very significant. Underestimation by manual method was possibly due to the shadow effect where the border was not defined, on the contrary segmentation and rule based classification helped in excluding the shadows more effectively.

The mean crown projected area estimates from each of the sensors, compared to the field-based measurements are summarised in Table 6.1.

Table 6.1.The crown projected area estimates by the two methods compared to the field measurements

Image source	Mean CA_{field}	SD CA_{field}	Mean image-derived CA	
			Manual vectorization	Segmentation
MS4100	210.96 m^2	136.39	194.52 m^2	182.87 m^2
ADS40			197.86 m^2	228.72 m^2
WV2			243.41 m^2	221.34 m^2

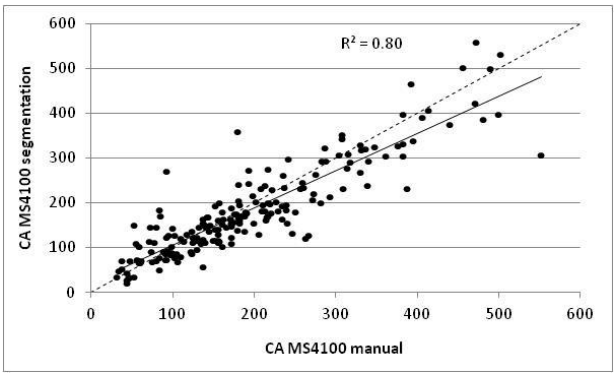

(a)

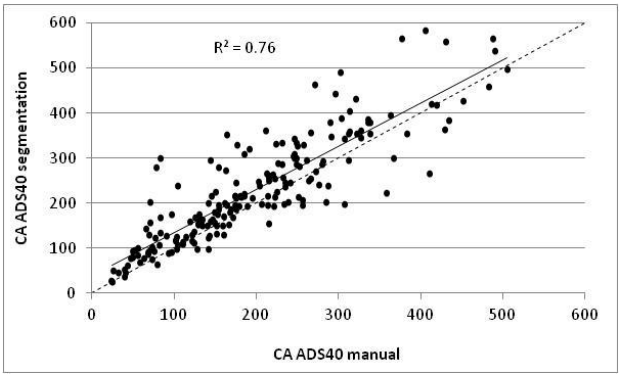

(b)

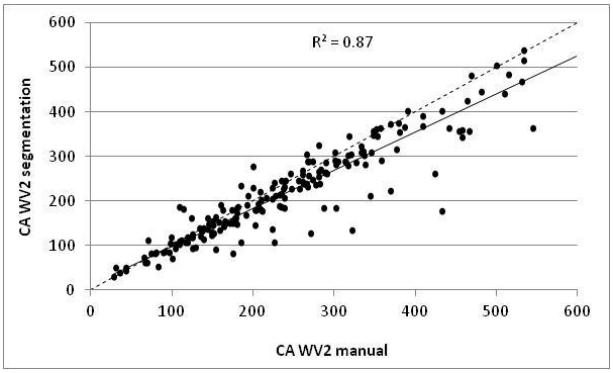

(c)

Figure 6.4. Scatter plots of the derived CA from each of the images using manual methods versus the segmentation based CA (a) MS4100, (b) ADS40, and (c) WV2 (n-172)

The conversion of image-derived CA (each sensor) into estimates of DBH for the candidate trees, using equation 1 (Niva et al 2014a) is given in Figure 6.5.

$$\ln(\mathrm{DBH}) = -2.40568 + 0.42616 \ln(\mathrm{CA}) \quad (1)$$

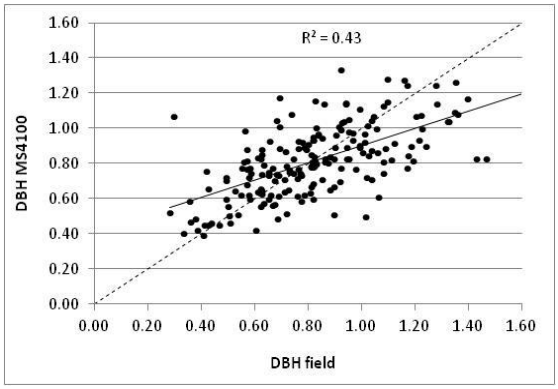

(a)

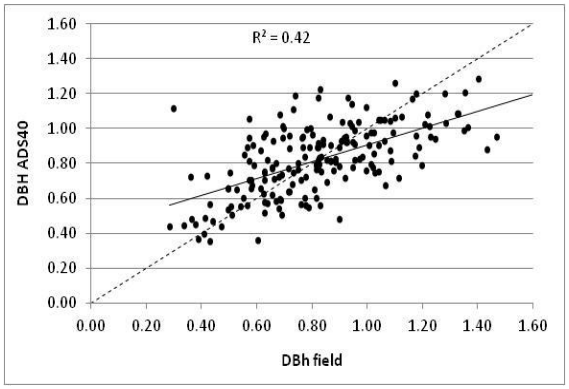

(b)

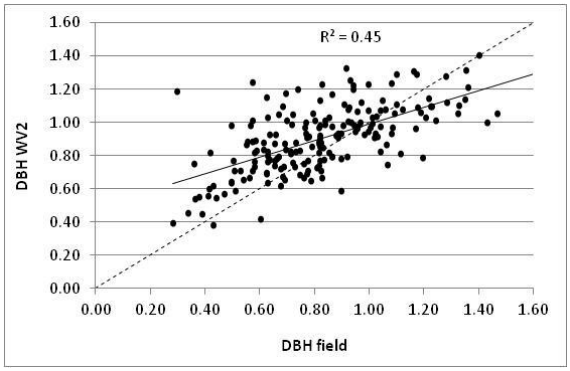

(c)

Figure 6.5. Scatter plots of the predicted DBH and the field-measured values for (a) MS4100, (b) ADS40, and (c) WV2. The image-derived CA was calculated using manual vectorization; n = 172.

Previous results (Chapter 2) have shown that either height or CA could be used to infer DBH. However the variance in DBH could be explained better by CA than height, hence CA is likely to provide better prediction than height. Assessment of the results in the present study showed that CA is an easily measured variable from high resolution remote sensing data and could be used for DBH estimation. The CA measured by these three sensors explained 40 - 45 % variance in DBH with MPE in the range of (error of 19-20% in all the sensors) which was slightly higher than the previous study where the MPE was ± 13 cm (error 17 %). However, this result was based on field based measurements only.

6.5 Conclusions

The allometric relationship between DBH and crown projected area (Chapter 2) made ways to CA estimations using high resolution remote sensing. This study discussed methods where CA can be extracted from high resolution remote sensing datasets of the order of sub metre resolution. An experimental analysis on sensor comparisons was performed and presented. The results of CA estimates from the two methods (manual and automatic) were close. The mean CA estimates from WV2 orthoimage was higher than the measurements from other two sensors and also than the field based measurements (211 m^2 versus 247 m^2 by manual vectorization method and 211 m^2 versus 221 m^2 by the segmentation method). Manually estimated crown projected area from both the ADS40 and MS1400 images were closer to the field based measurements (211 vs 195, in MS4100 and 211 vs 198 in ADS40) but underestimated, whereas automated method resulted in over and underestimations in ADS40 and MS4100 image, respectively. The higher mean value of crown projected area in WorldView2 image can be attributed to the orthorectified dataset (topographically corrected) where the shadow effect was minimized. However, this minimization of the shadow effect lead to slight overestimation of the crown projected area because the crown appeared flat and slightly bigger. ADS40 image helped in better demarcation of the crown projected area but led to the underestimation due to no distinct line of separation between the crown shadow and actual tree crown. MS4100 image resulted in lowest performance, though the spatial resolution was highest due to similar reasons. The most important point that comes out is that any sub metre resolution satellite imagery can be effectively used in CA estimations. Our outlined hypothesis that crown projected area estimations would be higher for high resolution images at least in this case, failed and the CA estimates, in fact, was found independent of the sensor resolutions. Therefore, the outcome supports that the expensive high resolution airborne datasets like MS4100 and ADS40 imagery which are usually expensive and lack temporal resolutions can be replaced by spaceborne sensor like WorldView2 for similar studies which would achieve similar accuracies. For study like this, the use of WV2 would be cost effective with less data acquisition time and available over a range of dates and time. The CA estimates from remote sensing also depends largely on the sun angle and in turn the shadow associated with the trees. This study can be further supported by using sophisticated and advanced remote sensing technology like LiDAR.

The intention of delineating CA from remotely sensed image was estimation of DBH from these measurements. The model for DBH prediction from the three sensors predicted DBH with MPE in the range of ±16 cm (error of 19-20% in all the sensors), as against the MPE of ±13cm (17 %) in case of field based measurements. This led us to conclude that identification of trees and extracting crown projected area for estimating DBH is a most promising technique. Field and image- derived crown projected area and DBH showed good correlations and in turn can be effectively used for estimating

other associated parameters like biomass and tree volume. The crown projected area estimates from remote sensing image was accurate (both by the method of vectorization and image segmentation) than the DBH estimates as evident from the R^2 values. This can be attributed to the fact that crown projected area, unlike DBH, is directly viewable by the sensor (Greenberg et al., 2005). Nevertheless it can be said that with the advances in availability of very high resolution remote sensing images and image analysis techniques, crown projected area can now be estimated with higher accuracy and the use of the model will help predict DBH using high resolution remote sensing datasets. Hence high resolution remote sensing can lead us to better understanding and prediction of forest characteristics and improvements in the forest ecosystem.

Chapter 7
Tree canopy measurements to infer canopy volume: A comparison of high resolution remotely sensed images and LiDAR

7.1 Introduction

The measurement of 3D volume is an important parameter in assessing the economic value of a tree (Gertner, 1991). A number of researchers have tried estimating biomass using biomass-volume relationships (example Fang et al., 1998). Tree volume measurements could include stem volume (volume of trunk from ground to tip), canopy volume or total tree volume (the sum of the former, i.e., volume of the trunk and the branches). Several allometric equations were developed that relate stem volume as well as the biomass of several tree components to diameter at breast height and/or to tree height (e.g., TerMikaelian and Korzukhin 1997; Eamus et al. 2000; Keith et al. 2000; Jenkins et al. 2004). This study determines canopy volume of trees in the study area.

Canopy volume includes the entire living canopy of a tree from the base of the crown to the upper edge of the crown and from the outer edge of the branch tips inward. It does not include dead branches, above or below the living portion of the canopy, and is an important parameter in the study of associated 'yield' estimations in horticulture (Tumbo et al., 2002). The conventional way of estimating the canopy volume of a tree canopy is by manual measurements of crown diameter and canopy height, and applies a number of assumptions appropriate to the 3D shapes of the crown. Because of varying crown shape, reach, extent and integral positioning of branches, it is difficult to calculate the tree derivatives and hence most published models have consolidated all the variations in tree crowns by using calculations for solid geometric objects (Coder, 2000). Canopy volume is generally calculated using a predefined solid geometric volume formula given in Eq. 7.1 (Coder, 2000).

$$\text{Canopy Volume} = \text{Crown Height} \times \text{Crown Diameter}^2 \times \text{Multiplier} \quad (7.1)$$

The choice of multiplier varies with respect to crown profile as different trees have different general crown profiles and crown shapes and hence will have different volumes (Frank, 2010). A number of researchers have calculated either stem volume or total tree volume assuming a certain geometric

shape. For example Cutini et al. (2013) calculated stem volume by applying Huber's formula assuming a cylindrical geometric shape and measuring the diameter at 0.5 m log length. The area of the top log was estimated assuming a conical geometric shape. Albrigo et al. (1975) computed the canopy volume of Valencia plots based on spheroid volume formula. Wheaton et al. (1995) studied Hamlin and Valencia orange cultivars by measuring trunk diameter and tree canopy, and canopy volume was calculated based on one half of an ellipsoid.

The relationships between canopy volumes with several tree components such as diameter at breast height and/or to tree height and crown profiles and crown shapes are used for canopy volume estimation. Figure 7.1 represents the work flow for the calculation of canopy volume based on tree characteristics measurements and a schematic of the measurable parameters is give in Figure 7.2.

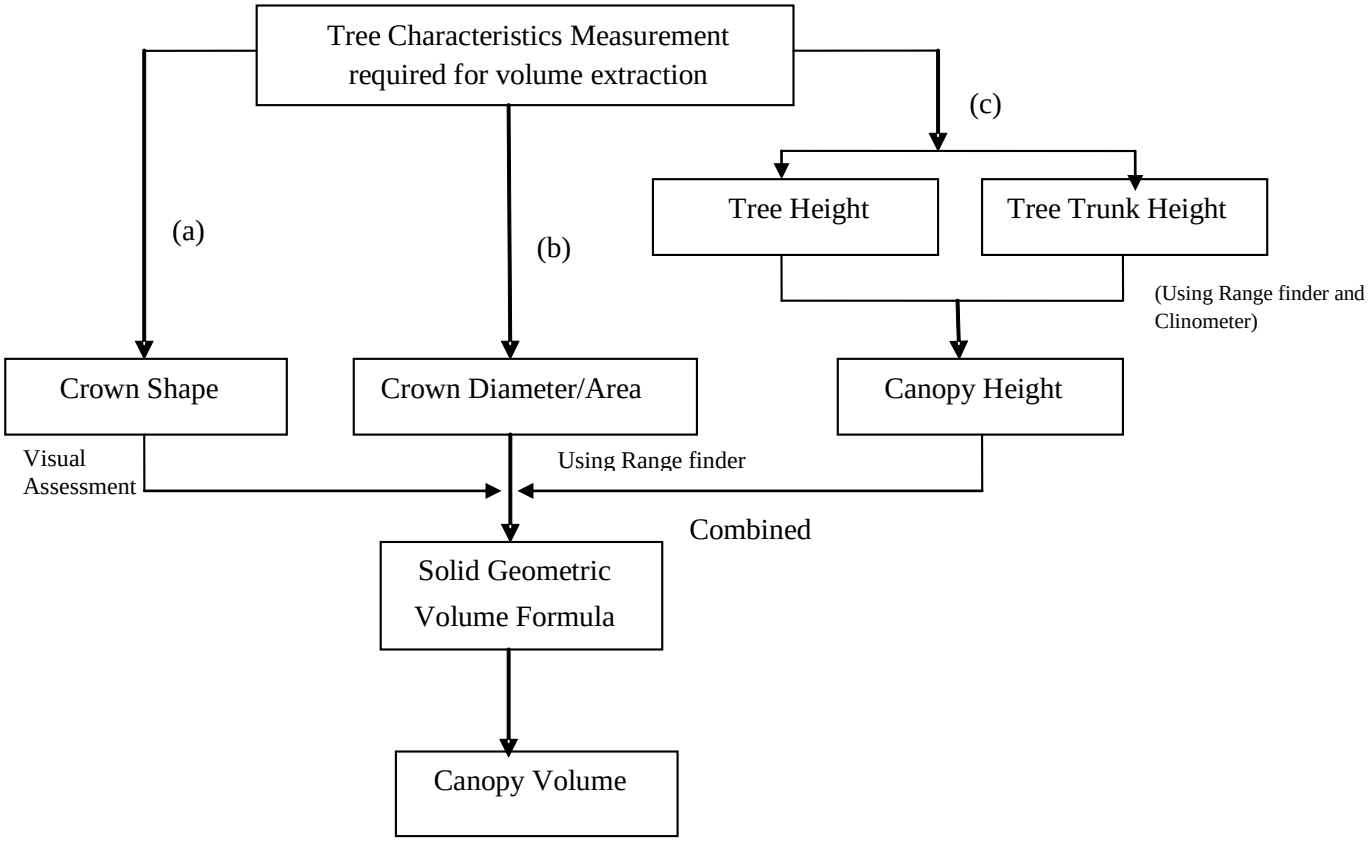

Figure 7.1. Flow diagram for canopy volume estimations

A schematic of the measurable parameters is given in Figure 7.2.

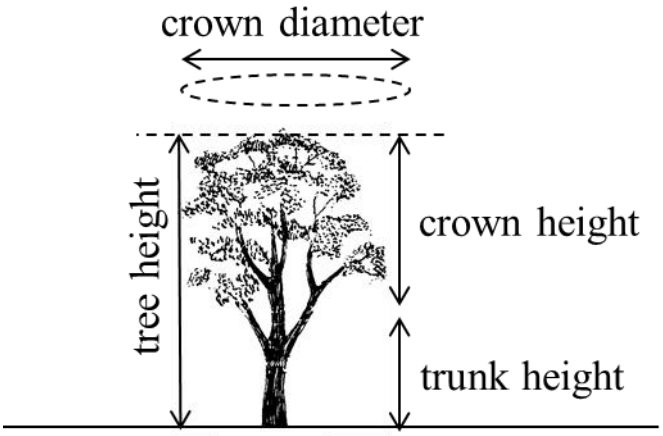

Figure 7.2. Schematic diagram indicating canopy dimensions required to estimate canopy volume

However, the development of canopy volume equation based on field based measurements is laborious and time consuming process. Lack of standardized approach further complicates the estimation. Therefore there is a need of much easier and convenient means for tree parameter measurements with similar accuracy. One technique that has attracted lot of attentions in recent years is through use of remote sensing data for tree parameters estimation and then for volume estimation. Optical data, LiDAR (light detection and ranging) and SAR (Synthetic Aperture Radar) are the three possible avenues for using remote sensing to infer canopy volumes. Optical data from both airborne and spaceborne platforms have been used to determine the relationships between tree height, crown diameter and crown cover derived from data and forest stand attributes (e.g., Gering and May 1995; Ozdemir, 2008).

The most direct remote sensing data for tree parameters and its attribute estimation is LiDAR, a distance (ranging) measuring technology that relies on the principle of 'time of flight'. Laser pulses are directed from a source (e.g., mounted on an aircraft) and a portion of the incident beam on the target is scattered back towards the source. High-speed detectors and electronics calculate the time of flight between the emission of the pulse and the return of the back-scattered component, and from this the distance (range) from the source to the target is calculated. LiDAR captures elevation information from a forest canopy as well as the ground beneath and can be used to assess complex 3D patterns of canopy and forest stand structure (e.g., Kini and Popescu 2004; Lefsky et al., 2002; Næsset and Økland, 2002). As LiDAR derived measurements such as tree height, trunk height, and canopy diameter etc., then can be used to estimate canopy volume based on formulae described in the Eq. 7.1. Few examples of LiDAR based canopy volume and biomass estimation along with other forest vegetation characteristics are: percent canopy cover (Nelson et al., 1984; Hyyppa et al., 2008; Lim et al., 2008; Lefsky et al., 2002), timber volume (Maclean and Krabill, 1986). Small-footprint LiDAR

systems are available commercially and research results on their potential for forestry applications are very promising (Næsset and Bjerknes, 2001; Holmgren et al., 2002; Næsset and Økland, 2002; Popescu, 2002; McCombs et al., 2003; Popescu and Wynne, 2003). Popescu et al., (2004) used LiDAR and multispectral data in forest to estimate tree volume and biomass in pine in Virginia USA. They found good estimations of biomass and tree volume in the case of pine with an RMSE of 29 mg/ha and 47.9 m^3/ha respectively. Naesset and Bjerkes (2001) reported that estimation of forest stand characteristics from airborne laser scanner data focused mostly on old forest stands or forests where the mean tree height exceeds about 15 m, and then estimated the mean heights of young forest stands with tree heights < 6 m and the stem numbers from small-footprint airborne laser scanner measurements such as canopy height and canopy density.

The other laser technology rapidly gaining attention is Terrestrial laser scanning. For forest applications where information at larger scales is required airborne LiDAR scanning seems inadequate. Terrestriall LiDAR on the other hand is implemented to obtain detailed information at the tree or plot scales. However, because of their short measurement range (up to 3 m), this technique is limited to measurements at organ or potted sapling scales under controlled conditions (Chambelland et al. 2008).

Although LiDAR derived tree measurements are more accurate and close to field based measurements, there are some drawbacks associated with LiDAR. With the existing technology LiDAR do have problems sometimes in seeing the ground and there are places with few or no ground returns, which make it hard to interpret. Hence while creating a DEM these places gets extrapolated this may cause the DEMs to be less accurate. In addition the principal challenge facing potential LiDAR users wishing to derive canopy volume measures for trees is cost and availability (Krogstad and Schiess, 2004).

Few studies explored the feasibility of 2D optical remote sensing data for tree parameter measurements and canopy volume estimation. For example, Ozdemir (2008) estimated tree volume from pan sharpened QuickBird imagery in open Crimean Juniper forests. Greenberg et al. (2005) presented a novel approach for generating regional scale above ground biomass estimates using hyperspectral remote sensing imagery. They related the area of shadowed vegetation to tree structural parameters, DBH and crown area. They measured the crown area assuming the crowns to be symmetric and found shadow method to be promising technique for estimating DBH and crown area.

Many studies have been carried out to estimate forest biophysical parameters using SAR radiometry and polarimetry. Gama et al.,(2010) established a relationship between volume and biomass with interferometric and radiometric SAR (Synthetic Aperture Radar) response from planted Eucalyptus

saligna forest stands, using multi-variable regression techniques. X and P band SAR images from the airborne OrbiSAR-1 sensor. The volume model developed showed that the stand volume was highly correlated with the interferometric height logarithm (Log10Hint), since Eucalyptus tree volume has a linear relationship with the vegetation height. This study represents the potential of SAR technology to help establish Eucalyptus forest inventory for large areas.

Numerous methods have been tested for tree parameters measurements and canopy volume estimations from remote sensing data with varying success. Chapter 3 has already demonstrated the ability to delineate tree canopies from remotely sensed imagery, while Chapter 5 described the ability to infer tree height from imagery and Chapter 6 explained the ability to infer tree crown projected area from remotely sensed imagery. These chapters explain the potential of image-based measurements of tree parameters from remote sensing data to infer canopy volume using Eq.7.1, provided the trunk height is given. Therefore, the question is whether in absence of a remotely derived measure of trunk height, can we infer canopy volume based on crown projected area and canopy diameter alone? Few studies have explored this possibility. For example, Ozdemir (2008) estimated tree volume by the method of regression from pan sharpened QuickBird imagery in open Crimean Juniper forests and found that volume can be predicted using just the crown projected area with an RMSE of 15.2 %. However, more studies are required in this area to support this.

This chapter therefore aims to compare the performance of two sensor systems (airborne LiDAR and spaceborne multispectral systems) and slightly different approaches for inferring tree canopy volume. The primary objective of this study is to investigate how well canopy volume in our remnant Eucalypt species can be estimated using LiDAR and satellite imagery, as compared to canopy volume estimated based on the field-based measurements as a benchmark. Also owing to the complexity associated with LiDAR data, the study explores the possibility of using multispectral image alone to estimate canopy volume given that canopy volume is a 3D tree derivative.

7.2 Materials and Methods

7.2.1 Study Area

The area chosen for the collection of laser and ground datasets was the region of the Newholme-Kirby property described earlier in Chapters 2-5. A subset of the study area, of approximately 200 ha was used (Figure 7.3 (insert)), limited in size by the LiDAR data acquisition footprint.

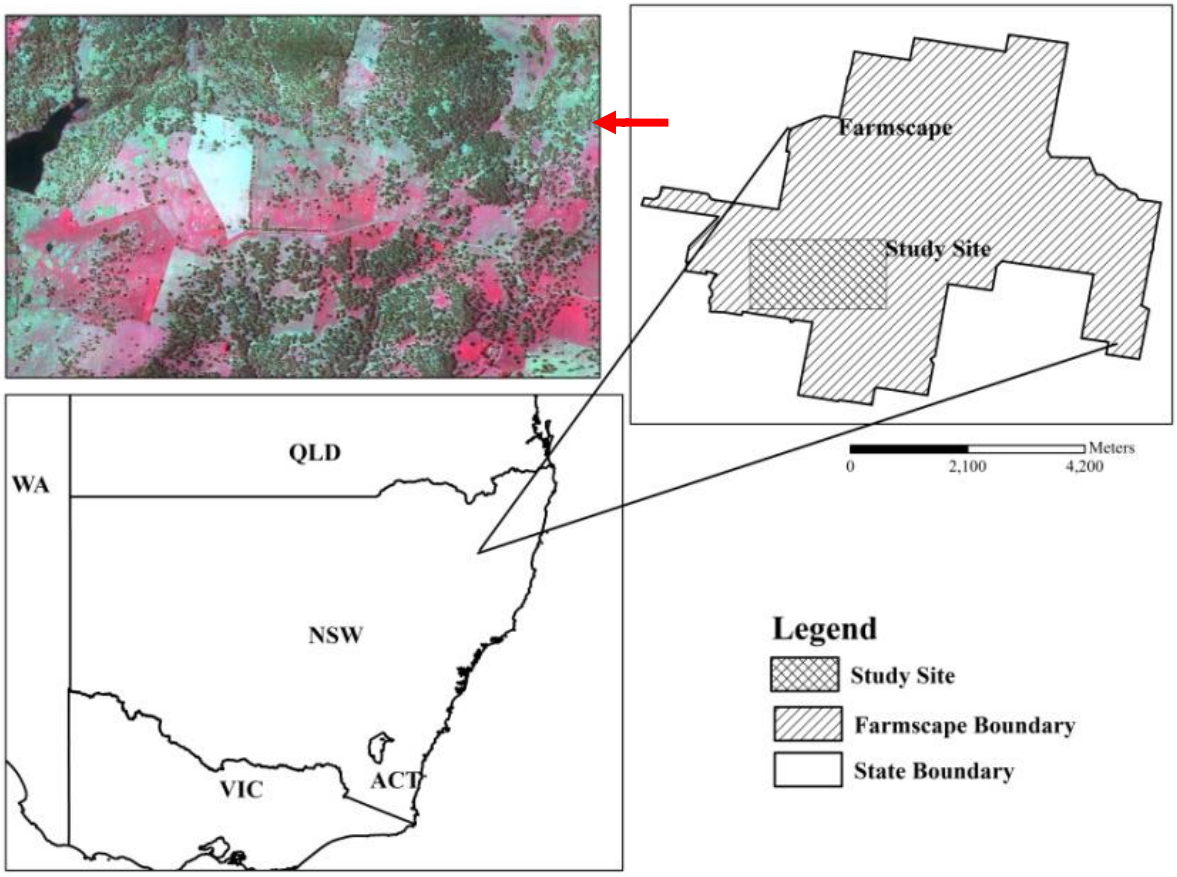

Figure 7.3. Location map of the study site in north eastern NSW, Australia.

7.2.2 Field measurements of canopy volume

Candidate single Eucalyptus trees were selected at random using the orthorectified imagery described in Section 2.4, with care was taken that the trees were well distributed across the study area. Field measurement was conducted in the month of September – December 2012. In order to establish the relationship between the crown variables with other tree parameters and canopy volume, 64 trees belonging to the five different Eucalyptus species were sampled. The number of samples for different species varied depending on the occurrence in the study area. The structural variables of Tree height (TH), Crown Diameter (CD) and Canopy Height (CH) were manually measured using a laser rangefinder (MDL LaserAce 300, Measurement Devices Ltd. Scotland, UK) and a measuring tape following the procedures outlined earlier in Section 2.4.3. The crown height was measured by first measuring the trunk height, and subtracting it from the total tree height (Figure 7.2). The crown diameter (CD_{field}, m) was measured using the protocol described in Chapter 2 (Verma et al., 2014a). The canopy volume (CV_{field}, m^2) was then calculated using Equation 7.1. Based on a visual assessment of the tree crowns in the study area, a parabolic profile crown 'multiplier' value of 0.3927 was deemed appropriate. The crown projected area (CA_{field}) was calculated from the crown diameter values using the equation in Verma et al. (2014a) (Chapter 2, Equation 2). A regression equation was then developed between canopy volume (CV_{field}), and crown diameter (CD_{field}) and crown projected

area (CA_{field}) parameters to allow subsequent determination of canopy volume from the satellite data which was unable to provide measurements of canopy height (discussed later in Section 7.2.3).

7.2.3 LiDAR data acquisition and post-processing

The Airborne Laser Scanning system used for the project was the Trimble Harrier 68i/G1 system flown on June 1, 2013. It consists of a Riegl LiDAR scanning instrument, Applanix POS/AV 410 Inertial Motion System and 12 channels and a dual frequency GPS. The full waveform LiDAR data collected has the following parameters (Table 7.1):

Table 7.1. LiDAR data acquisition parameters

Parameter	Value	Unit
Scanning Angle	60	degrees
Flight Speed	216	$kmhr^{-1}$
Flight Height	375	metres
Scan Rate	192	Hz
Pulse Rate	400	kHz
Swath Width	433	metres
Swath Overlap	37	%
Along Track Point Spacing	0.31	m (along track)
Across Track Point Spacing	0.31	m (across track)
Outgoing Pulse Density	10.26	m^{-2}
Cumulative Pulse Density	17.86	m^{-2}
Calculated Spot Footprint	0.19	m

The acquired LiDAR data were provided in LiDAR Exchange Format (LAS), having first been classified as ground and non-ground points by the data provider using proprietary software (Terrascan). An intensity image was created from the point clouds. The selected individual trees measured in the field were then identified in the point cloud data. The tree height and trunk height was manually measured for each tree using the software FUSION/LDV (Robert J. McGaughey, Pacific Northwest Research Station, Version 3.10, Build date May 16, 2012) (Figure 7.4). The canopy height was then calculated from the difference between the tree and trunk heights.

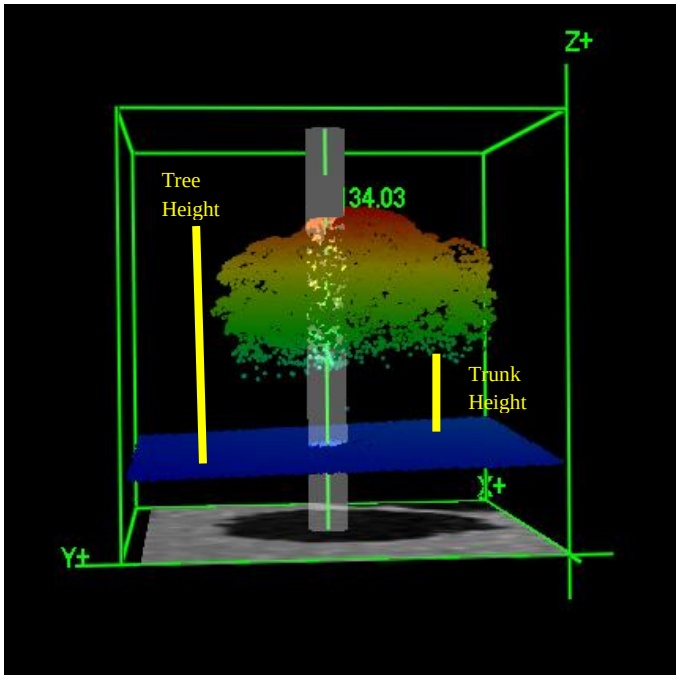

Figure 7.4. Tree parameters (total tree height and trunk height) from FUSION/LDV software. The colours green, yellow and red represents the canopy at different heights. Blue represents the ground height.

The automatic extraction of crown parameters from LiDAR was a two step process involving 1) Canopy Height Model generation (CHM), and 2) Segmentation of the CHM 'image' into homogenous objects representing individual tree canopies. CHM generation requires two grid inputs namely a Digital Terrain Model (DTM) and a Digital Surface Model (DSM). DTM refers to a digital representation of topographic surface where the height values in the terrain were known (Dash et al. 2004). DSM was a representation of features above the terrain. The canopy height model, also referred to as a normalized digital surface model (nDSM), with a vertical resolution of 1m was created by subtracting the DTM from the DSM. The resolution of CHM was important as the tree height information extraction from canopy height model largely depends on the accuracy of the height model. The processing was done using ArcGIS version 10. The canopy height model was used to extract trees using the method of image segmentation. The software eCognition (eCognition Developer 8, Munich, Germany, GmbH) used for image segmentation and classification offers a wide range of segmentation algorithms suited for an array of datasets. The derived canopy height model was a grid which was represented as a single band image, where the objects appeared partitioned into lighter and darker areas. A 'contrast split' segmentation algorithm was employed for tree extraction which was later was refined based on the tree heights (Figure 7.5).

The extracted tree polygons were exported to ArcGIS 10 and in accordance with the field based measurements (Section 7.2.2), the six diameters were measured and the average used to specify crown diameter (CD_{LiDAR}).

Canopy heights were estimated by subtracting trunk height from tree height. The canopy volume (CV_{LiDAR}) was then calculated using Equation 7.1 with the same 'multiplier' as used for the field-based measurements.

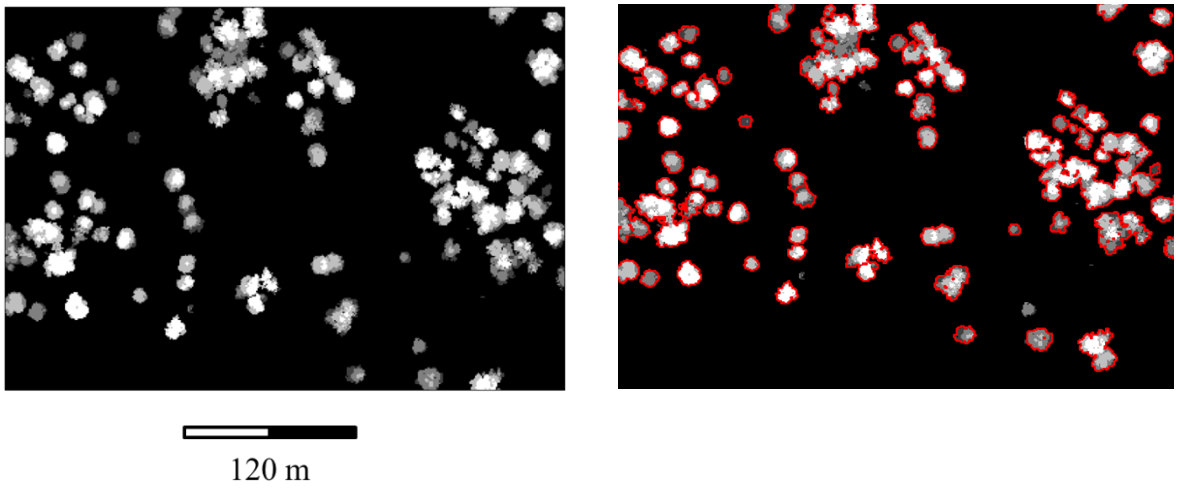

(a) **(b)**

Figure 7.5. An example of the (a) derived LiDAR canopy height model (CHM) and (b) the segmentation results.

7.2.4 Delineation of tree attributes from WorldView2 data

A multispectral, PAN sharpened, WorldView2 image (8-bit) of January 1, 2012 was acquired with a spatial resolution of approximately 50 cm in four spectral bands, Band 1 (NIR 0.7-1μm), Band 2 (Red 0.6-0.7μm), Band 3 (Green 0.5-0.6μm) and Band 4(0.4-0.5 μm). The image reference system was WGS 84 UTM Zone 56 S projection system.

The crown projected area for each of the trees (CA_{WV2}) was determined following the process described in Section 6.3; calculated by the manual method of onscreen digitization/segmentation of the canopies (ArcGIS version 10) and counting of the canopy pixels, assuming a pixel dimension of 50 cm x 50 cm. The crown diameter (CD_{WV2}) of the individual trees was then determined by first identifying and then measuring the length of the major and minor axes of the individual tree canopy polygons, and then calculating the average of the two.

In order to estimate canopy volume for the WorldView2 imagery (CV_{WV2}), the regression equation developed between on-ground measurements of canopy volume (CV_{field}), and crown diameter (CD_{field}) and crown projected area (CA_{field}) (Section 7.2.2) was applied to the derived values of CD_{WV2} and CA_{WV2}.

7.2.5 Evaluating the performance of the two techniques

The derived canopy volumes for each remote sensing method (CV_{LiDAR}, CV_{WV2}) were compared to the field-measured values (CV_{field}) and a mean prediction error (MPE) given by $MPE=\overline{|CV_{predicted}-CV_{actual}|}$ calculated.

7.3 Results and Discussion

7.3.1 Field measurements of tree parameters

Summary statistics of the measured trees are given in Table 7.2.

Table 7.2 Summary statistics for single trees from the field measurements; n = 79 is the number of trees used in the model development.

Tree characteristics	Min	Max	Mean	Std.Dev
crown diameter (CD_{field}, m)	6.8	30.5	15.2	4.9
crown projected area (CA_{field}, m)	36.3	731.8	210.4	129.1
tree height (m)	12.7	42.8	21.3	5.3
Canopy height (m)	8.8	30.6	16.1	4.1
canopy volume (CV_{field}, m^3) (Equation 7.1)	217.9	9040.8	1840.2	1533.1

Scatter plots of canopy volume (CV_{field}) versus crown diameter (CD_{field}) and crown projected area (CA_{field}) are given in Figure 7.6 and Figure 7.7, respectively, along with the best-fit, polynomial regression curves. The derived regression equations corresponding to these curves are given in Table 7.3.

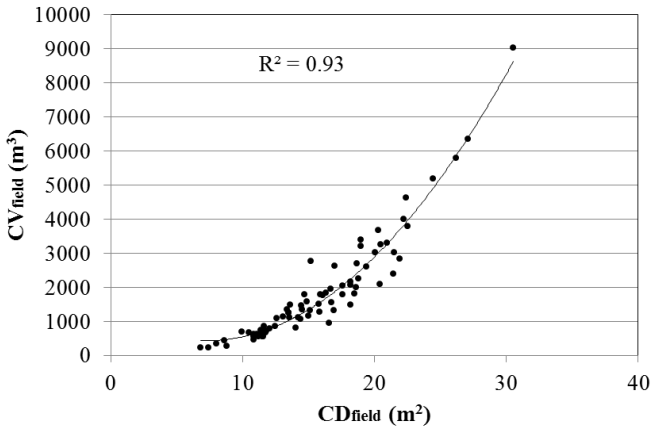

Figure 7.6. Scatterplot between canopy volume (CV_{field}), as calculated using Equation 7.1, and measured crown diameter (CD_{field}). The solid curve is the best-fit, polynomial regression equation.

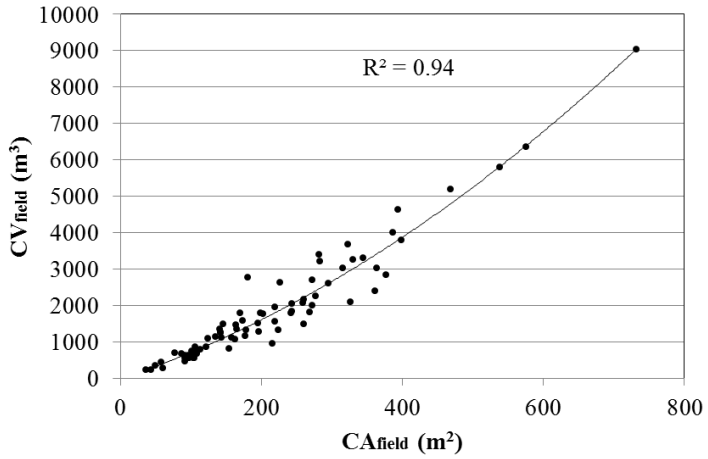

Figure 7.7. Scatterplot between canopy volume (CV_{field}), as calculated using Equation 7.1, and measured crown projected area (CA_{field}) derived from field measurements. The solid curve is the best-fit, polynomial regression equation.

Table 7.3. Derived best-fit regression parameters for calculating canopy volume (CV_{field}) from Equation 7.1 using field measurements of crown projected area (CA_{field}) and crown diameter (CD_{field}). Multiplier value = 0.3927 (n = 79).

Equation	R^2	F-stat	P
$CV_{field} = 0.008 \times CA^2_{field} + 6.5673 \times CA_{field} - 25.199$	0.93	993.0	<0.0001
$CV_{field} = 15.11 \times CD_{field}2 - 218.58 \times CD_{field} + 1222.6$	0.94	415.6	<0.0001

Both Figures 7.6 and 7.7 and the regression statistics on Table 7.3 indicate the canopy volume of the candidate Eucalyptus trees can be inferred using crown diameter or crown area, without the need for measuring canopy height and this bodes well for using remotely sensed imaging systems.
The application of the two regression equations in Table 7.3 to estimate the canopy volume is depicted in the scatter plots of Figure 7.8 (a,b). Here the predicted canopy volumes (CV_{WV2}) are compared against the field measured values, the latter including the additional crown height parameter in Equation 7.1.

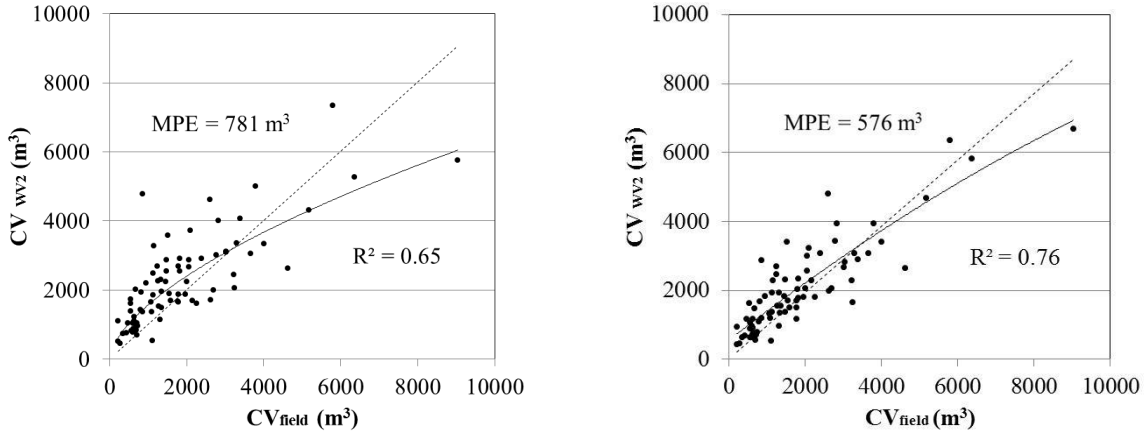

(a) (b)

Figure 7.8. Scatterplots of canopy volume from WV2 using (a) crown projected area (CA), and (b) crown diameter (CD) as the predictor variable, and field measurements. The dashed lines are the 1:1 equivalence between measured and predicted values and the solid lines the best-fit regression curves (power and polynomial, respectively).

Both scatterplots include a 1:1 equivalence line (dashed line) and a 'best fit' regression curve. The accuracy of using the WorldView2 imagery to infer canopy volume via CA and CD is different, as depicted in Figure 7.8 (a) and (b), respectively. A MPE of 781.03 m^3 (error 42 %) was observed when using CA as the predictor variable, whereas a comparatively lower MPE (MPE 575.5 m^3, 31% error) was observed with crown diameter (CD) as the predictor variable. Both scatter plots include a regression curve; a power law explains 65% of the variance between the field and WV2-derived canopy volume when using crown projected area as the sole variable, whereas a second order polynomial relationship between the field and WV2-derived canopy volume when using the crown diameter as the variable explains 76% of the variance. Both parameters yield, on average, and overestimation of the canopy volume compared to the field measurements and this is most likely due to the visual classification of mixed, boundary, pixels as canopy. As the imagery was orthorectified it was often difficult to determine whether the shadow fringes observed in the imagery were parts of the crown, or that cast upon the underlying ground surface. Consequently the shadow fringes were allocated as part of the tree canopy. In both cases CA and CD would then be overestimated, hence yielding a higher CV value. It is likely that the CA-derived CV_{WV2} estimates are higher than the CD-derived CV_{WV2} the because of the additive effect of the erroneously included pixels in calculating CA. The canopy diameter measure is at least an average of the numerous transect measures. Ideally an objective classification procedure would apportion sub-pixel dimensions according to the level of mixing, and this is a recommended subject of further work. At higher canopy volumes (> ~4000 m^3) both techniques tend to underestimate the canopy volume, although there is considerable spread in the predicted versus actual values for these larger canopies.

A scatterplot of the LiDAR-dervied canopy volume versus the field measured CV is given in Figure 7.9. The parameter CV_{LiDAR} is calculated using Equation 7.1 and both the derived measurements of crown height and crown diameter from the LiDAR data. Even though a lower MPE was observed when crown volume was estimated using the LiDAR measurements (490.8 m^3, 26 % error), there does appear to be a systematic underestimation of the canopy volume, especially for the larger canopy volumes (> ~ 2000 m^3).

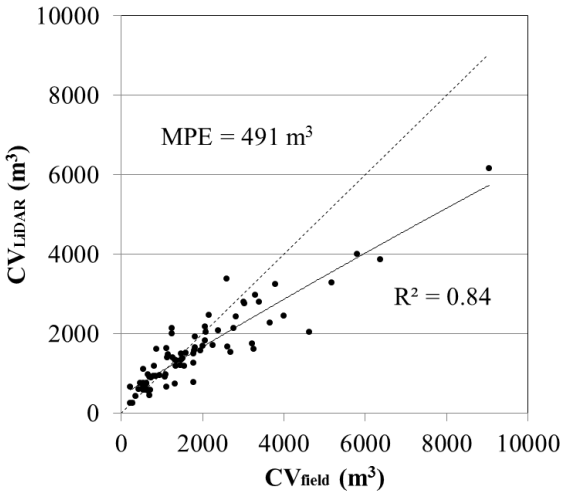

Figure 7.9. Scatterplot between canopy volume predicted using the LiDAR-derived values of crown height and crown diameter (Equation 7.1) and the field measured values. The dashed line is the 1:1 equivalence between measured and predicted values and the solid line is the best-fit regression curve (polynomial).

The individual parameters, extracted from the LiDAR data, used to calculate the CV_{LiDAR} values are plotted in Figures 7.10 (a) and (b).

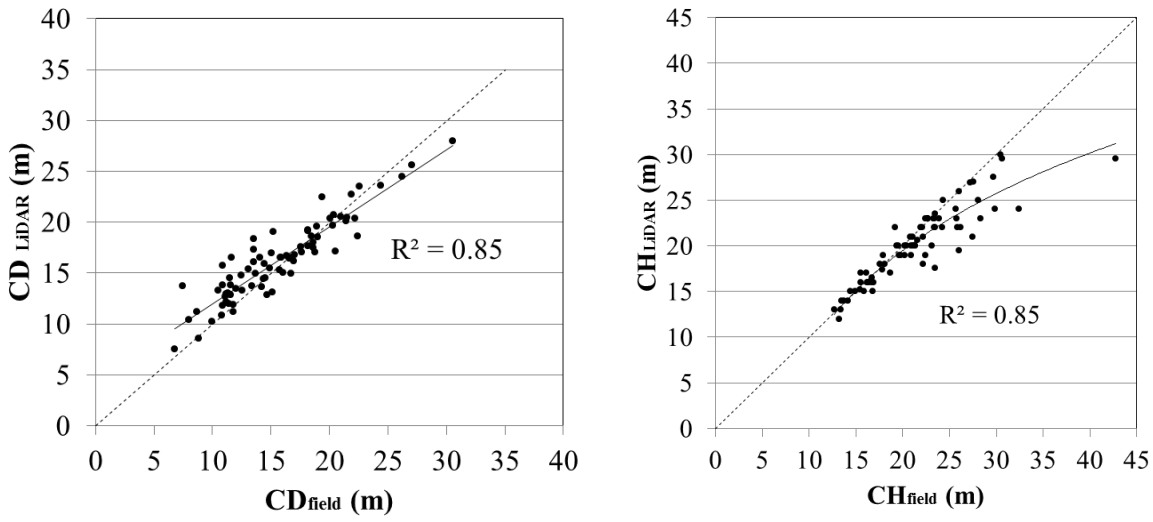

(a) (b)

Figure 7.10. Scatterplot between (a) LiDAR-derived crown diameter and field measurements, and (b) LiDAR-derived crown height and field measurements. The dashed lines are the 1:1 equivalence between measured and derived values and the solid lines the best-fit regression curves (liner and polynomial, respectively).

Many studies have shown to achieve promising results of lidar systems for assessing single tree heights (Hyyppä and Inkinen, 1999; Andersen *et al*., 2001; Hyyppä *et al*., 2001a and 2001b; Persson *et al*., 2002; Brandtberg *et al*., 2003; Holmgren *et al*., 2003; McCombs *et al*., 2003; Popescu *et al*., 2003; Holmgren and Persson, 2004; Popescu and Wynne, 2004; Yu *et al*., 2004; Roberts *et al*., 2005) and forest plot or stand heights (Næsset, 1997; Magnussen and Boudewyn, 1998; Magnussen *et al*., 1999; Means *et al*., 2000; Næsset and Bjerknes, 2001; Næsset and Økland, 2002). However, studies from Rönnholm *et al*., 2004 and Huang et al., 2009 have shown that tree heights are typically under estimated by small footprint laser scanning system due to varied number of reasons like (a) variability in the density and coverage of laser pulses, (b) differences in the algorithms used to obtain the canopy height model, (c) the amount and height of understory vegetation obscuring the ground surface, (d) differences in algorithms used to calculate the bare ground elevation, (e) the sensitivity of the laser system and the algorithms used for signal processing, and (f) lastly the tree shape and tree species.

Analysis of results in the present study (Figure 7.10) shows that both parameters (Crown diameter and canopy height) used in Equation 7.1 tends towards underestimating at higher values. Crown diameter shows a slight underestimation whereas canopy height shows significant underestimations especially at height above 20 m resulting in underestimation of canopy volume $CV_{LiDAR\ versus}$ CV_{field}. Given the diameter value is squared in Equation 7.1 , even that little bit of underestimation is exaggerated too.

The present study uses full waveform LiDAR with a point density of 10 per m^2. Literature review suggests this point density to be good enough for height and other parameter estimations. Therefore, the reasons in this case for underestimations can be attributed to the flying height as well as point spacing which in this case are 0.31 m along and across track which may have had an effect. Other factors that influence the crown diameter and canopy height measurements may be the number of pulses actually hitting the tree edge and understory which would fail to provide a clear demarcation between the trunk height and the start point of the tree canopy.

7.4 Conclusions

Field based measurements provides the best estimate for any forest characteristics measurements but it is often expensive and labor intensive, hence it was felt that there should be a practical alternative to the field based estimations. In this line canopy volume for single eucalyptus trees were estimated using basic crown parameters like crown diameter and canopy area extracted from image based remote sensing systems like WorldView2. The results from WorldView2 data were found impressive and beyond doubt it can be positively said that optical remote sensing can also act as a possible avenue for measuring three dimensional attributes like canopy volume. This remote sensing system can thus be looked as viable alternative to field and LiDAR based assessments for determining canopy volume.

It was not surprising that LiDAR performed well and LiDAR measurements agreed very well with the field based measurements. The LiDAR based measurement method estimated tree heights with an MPE of 1.44 m (error of 6.5%), and estimated canopy volume with an error of 26% which was promising and consistent with other LiDAR based studies, for example Maltamo et al., (2004) estimated timber volume using LiDAR with RMSE being under 30%. McInerney et al., (2010) estimated canopy height from LiDAR and medium resolution image combined and found the RMSE to range from 2 – 31% in two separate studies. Though better performance of LiDAR cannot be ruled out but, but due consideration should be given to the high price and complexity associated with the acquisition and processing of these datasets which makes them not so feasible. In addition it can be argued that even though, LiDAR measurements were significantly accurate few samples did differ from the field based measurements. Reasons, since canopy height was estimated by measuring the total tree height and trunk height there is a chance of error propagation which explains the percentage error in canopy volume estimations using LiDAR.

The model based results using WorldView2 appeared quiet encouraging and can be considered a direct way of estimating canopy volume; however, the predictability of the model could potentially be enhanced by incorporating terrain characteristics like slope, aspect, rainfall etc that could also have an impact on the overall volume estimates which can be the topic for future study. The automated tree crown measurements like crown projected area and crown diameter by segmentation methods offered

greater capabilities to LiDAR and multispectral image data analysis. The study can be extended to future research wherein different resolution remote sensing datasets can be tested against the volume estimations. The overall outcome of this study strongly supported the hypothesis that high resolution remote sensing data can be effective in canopy volume estimations without relying on expensive datasets like LiDAR.

Chapter 8
Remote Sensing based Stem Density measurements in Tree Clusters for DBH estimation: comparison of techniques

8.1 Introduction

This study follows on from the results of Chapter 2 which indicated that both tree height and crown projection area can be used to infer diameter at breast height (DBH) for single trees and tree clusters. In this earlier work, tree clusters were defined as groups of trees (n = 2-30) growing in proximity. The average DBH of the clusters, ranging in density from 38 to 536 stems per ha were predicted using average crown area per stem as the predictor variable (Chapter 2, Figure 2.8, Niva et al., 2014a). However, in order to be able to apply the relevant allometric equation (for example Table 2.5 or 2.6 in Chapter 2) to tree clusters in a situation where it is not possible to clearly delineate the number of tree stems within the cluster (for example as inferred from the shape of the canopy envelope) then additional information on the number of stems within the canopy envelope is required. Consequently, this chapter seeks to determine whether LiDAR data can be used to provide this extra information, for example following Popescu et al. (2003), for the clusters of Eucalypt species occurring in the farmscape chosen for this thesis.

A number of algorithms have been developed to delineate individual tree crown and tree stems using LiDAR. Local maximum filtering (Wulder et al., 2000; Popescu et al., 2002) and watershed segmentation (Wang et al., 2004) are two of the widely used techniques for such studies. The local maximum filtering method, in case of optical image, assumes tree apex as the highest point of reflectance of a tree crown, while with LiDAR data, it assumes that among the laser hits for a tree crown the highest laser elevation value represents the tree apex. Successful identification of the tree location using the local maxima technique, however, depends on the careful selection of the filter window size. Inverse watershed segmentation, commonly referred as watershed segmentation, is the most common method applied to determining locations of individual tree crowns using a Canopy Height Model (CHM). Tree identification process involves the segmentation of inverted raster canopy surface into the equivalent of individual hydrologic drainage basins (Andersen, 2009). The inversion step helps in separating the CHM into distinct tree polygons with raster crown diameter and height values.

Using the above mentioned algorithms tree stems can be automatically detected based on certain pre-defined criteria. However, the primary requirement is generation of a CHM, also called normalized digital surface model (nDSM), which aids in estimation of tree stems in a cluster. The CHM is generated from two image grids, namely a Digital Terrain Model (DTM) and a Digital Surface Model (DSM). The DTM refers to a digital representation of topographic surface where the height values in the terrain are known (Dash et al., 2004) and is extracted from the last return signal from the dynamic time of flight data generated by the LiDAR profile. The DSM is a representation of features above the terrain, and represents the mean sea level (MSL) elevations of the reflective surfaces of trees, buildings, and other features elevated above the "Bare Earth". The LiDAR derived CHM plays a very important role in forest studies especially when attributes of interest is three dimensional in nature like biomass, volume, tree height etc. Numerous researchers have successfully used LiDAR derived CHM's for estimating tree attributes with significantly high accuracy. For example, Jung et al. (2011) estimated crown variables like crown base height, tree height, crown area and crown geometric volume using airborne and terrestrial laser scanners (ALS and TLS) and concluded TLS to be performing better than ALS. In another study, Hunter et al. (2013) estimated biomass using tree heights measured from LiDAR derived CHM across Brazilian Amazon and concluded LiDAR to be performing well.

Although the above mentioned techniques (local maxima filtering and watershed segmentation) have been used successfully for estimation of tree attributes with varying accuracies, the selection of one over another is always important for a desired outcome in given study. In such conditions, it is often the case when the relative performances of two techniques are compared and the choice is made with one with superior outcomes. The current study compares the performances of these methods in determining stem numbers using LiDAR data. A third method using LiDAR point clouds has also been tested to explore the possibility of alternative to above two techniques. Three different, freely available software packages, corresponding to one of the three algorithms are tested. These are: TreeVaW (based on local maximum filtering), SAGA GIS (based on watershed segmentation) and Fusion/LDV (based on the LiDAR point clouds).

A number of studies have been carried out using these algorithms in tree attributes determination. For example, Cao et al. (2012) extracted forest structural parameters based on LiDAR data using local maximum filtering technique and found only little deviation between the extracted and measured tree locations. Ke and Quackenbush (2008) used three different algorithms for tree crown detection namely marker controlled watershed segmentation, region growing and valley following approach. They concluded that different algorithms could be employed in different applications. For example marker-controlled watershed segmentation which was based on the assumption that tree tops have highest reflectance and are located at or near the centre of the crown, could be used in delineating

trees with circular shape. Edson and Wing., (2011) studied individual stem location and biomass measurements using three methods namely FUSION, watershed segmentation (ARCGIS) and TreeVaW. They concluded all the methods to be performing well, however watershed segmentation was able to detect smaller trees better than TreeVaW and FUSION.

This study investigates the three algorithms described earlier, namely TreeVaw, SAGA GIS and FUSION for LiDAR data analysis and compares the stem numbers detected by each method with the field based measurements. IN doing so, this study completes the hypothesis originally posed in Chapter 2 (Verma et al., 2014a) that remote sensing can exclusively be used for DBH estimation in tree clusters.

8.2 Materials and Methods

8.2.1 Study Area

The study area was the same used in Chapter 7 (Figure 7.3).

8.2.2 Tree measurements

The trees used in this analysis were the same clusters of eucalypt trees described earlier in Chapter 2 (Verma et al., 2014a). However not all of the 52 tree clusters were used owing to the limited data capture area of the LiDAR system. A total of 7 tree clusters were utilized for this particular analysis, ranging from 3 to 15 stems and densities ranging from 15 stems per ha to 52 stems per ha.

8.2.3 LiDAR Data

The same LiDAR point data described earlier in Chapter 7 (Section7.2.2) was also utilised for this study. The LiDAR data encompassed an area of approximately 200 ha, consisted of mixed Eucalyptus species with dimensions summarized in Table 8.1.

Table 8.1. Physical characteristics of clustered trees; n is the number of tree clusters

Tree cluster species	n	Min	Max	Mean	SD
Number of stems	7	3	15	5.71	4.34
Stems per ha	7	15	52	37	13

Using the raw point dataset, the following interpolations were created: DTM from the first return signal, digital surface model (DSM) from the latest return signal and, by the subtraction of the DTM from the DSM, the CHM, as discussed earlier in Section 7.2.2.

8.2 LiDAR data processing for tree stem extraction

A canopy height model, CHM, or nDSM as it is commonly referred, with a vertical resolution of 1m was created by subtracting the DTM from the DSM. The CHM was generated using ArcGIS version 10 (Environmental Systems Research Institute, Inc., Redlands, CA).

TreeVaw (1.1) implements the CHM processing software in Interface definition Language (IDL) to identify trees based on the local maximum filtering technique that uses a search window of variable size (Kini and Popescu, 2004). The program was designed for conifer forest applications and is based on the relationship between crown diameter and height. The software program delineates trees by deriving an appropriate circular size search window to find tree tops from the height model based on the above mentioned relationship. For TreeVaW the CHM in TIFF file format was used (since TreeVaW uses ENVI image format). Defining parameters such as minimum crown diameter, maximum crown diameter, and minimum tree height were constrained to values based on the field measurements. For example any CHM values less than 7 m were discarded as 'trees clusters' as they were understorey vegetation. The equation pertaining to the crown diameter and tree height relationship, Crown Diameter = 5.9133 + 0.4489 * Tree Height (from previous work, Niva et al., 2014a) was used since TreeVaW also allow users to specify the crown height relations as per the area and species under consideration. The minimum crown diameter was set to 3.5 m and the maximum to 30 m. The output image consists of the X and Y locations of each of the detected trees within a cluster along with the heights and radii of individual crowns (Popescu and Wynne, 2004). The X and Y locations of the detected trees were converted into point locations and overlaid on the image using ArcGIS 10.

SAGA GIS (version 1.1.1, Department of Physical Geography, Göttingen) focuses on Digital Elevation Models (DEM) and Terrain Analysis to extract information on the tree stem numbers within clusters. The grid analysis algorithm in SAGA GIS, such as Gaussian Filter, and Watershed Segmentation helps extract information on tree numbers. The algorithm is one of the most common methods applied recently for tree crown identification which separates the CHM into distinct tree polygons with crown diameter and height values. The result in form of an output shape file gives optimum stem numbers in a cluster. Since the output is in shape file format it is easier to perform overlay operations directly in ArcGIS 10. The first step in counting trees using SAGA also involves creation of CHM by subtracting DTM and DSM followed by smoothening of the height model. The segmentation is performed on the smoothed height model, which simultaneously creates a point layer

based in the number of trees detected. This later can be refined by selecting the trees above a certain height (above 7m in the present study).

FUSION/LDV (version 3.10, Pacific Northwest Research Station) has two interfaces: FUSION and 'LDV'; the latter being a LiDAR data viewer and uses LiDAR point clouds to determine stem numbers. Among the three algorithms, TreeVaW and SAGA GIS methods automatically delineate the crowns while FUSION/LDV requires user to manually locate the stems from the LIDAR point cloud data. The basis of FUSION is the LiDAR point clouds. The point clouds classified as ground and non ground points by the data provider were taken into FUSION directly for further analysis. Trees were displayed based on the unique identification numbers which were assigned to each tree during field sampling. Each tree was selected manually and tree parameters were measured in LDV using a measurement marker. Tree stems were measured by counting the number of elevated crown in each cluster. There are a number of parameters available which can be set before the tree measurements, like the return numbers, the tree locations etc. The field measured stem numbers and those determined by the three image-based methods were compared.

8.3 Results and discussion

The final outputs generated by the three algorithms are given in Figures 8.1 through 8.3. A point coverage generated from TreeVaW representing the tree location is shown in Figure 8.1. The segmentation results from SAGA GIS and stems numbers extracted using these segments are shown in Figure 8.2 whereas Figure 8.3 shows the trees in the cluster as rendered in FUSION/LDV.

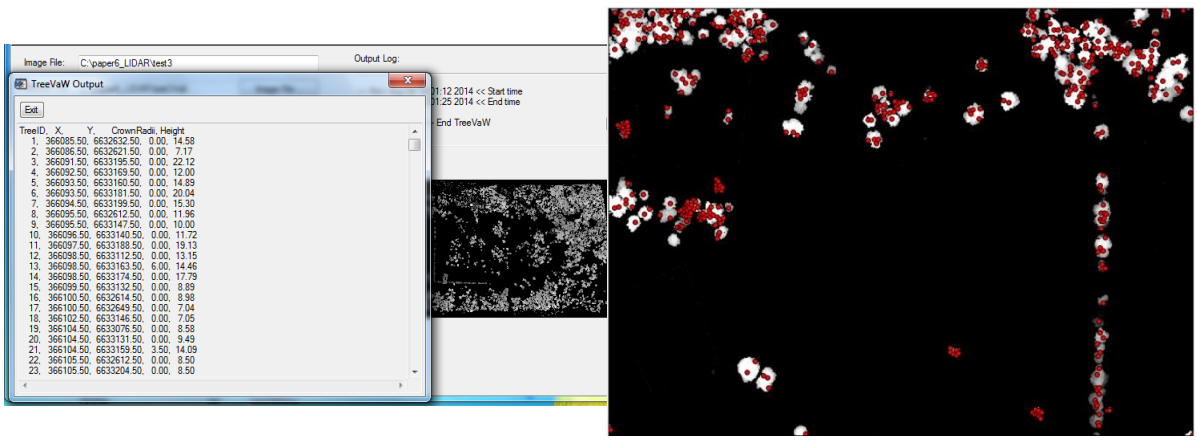

(a) (b)

Figure 8.1. Tree crowns in a cluster as detected from TreeVaW algorithm. (a) The tabular output and (b) detected trees overlaid on the canopy height model

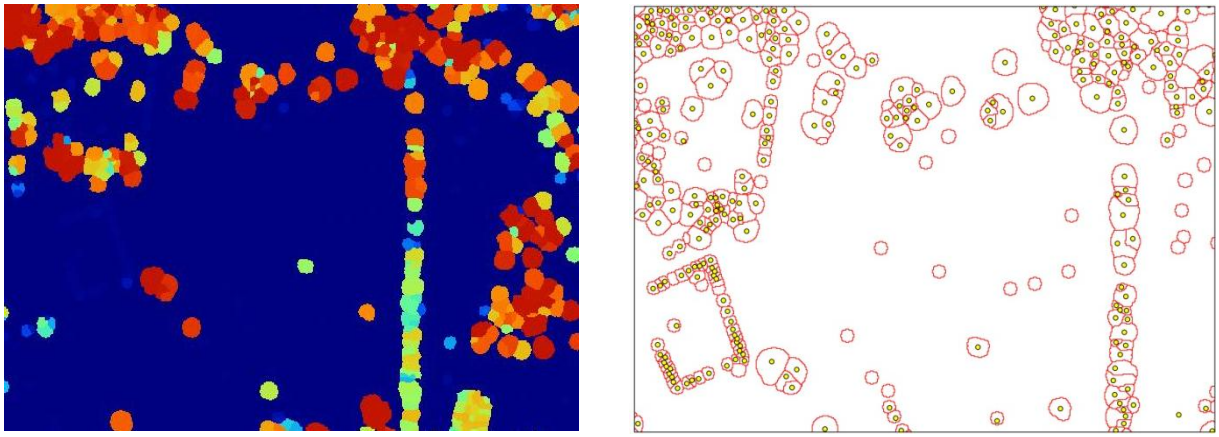

(a) (b)

Figure 8.2 Tree crowns in a cluster as detected from SAGA GIS software. (a) The segmentation Output and (b) the segments with each point representing a tree stem

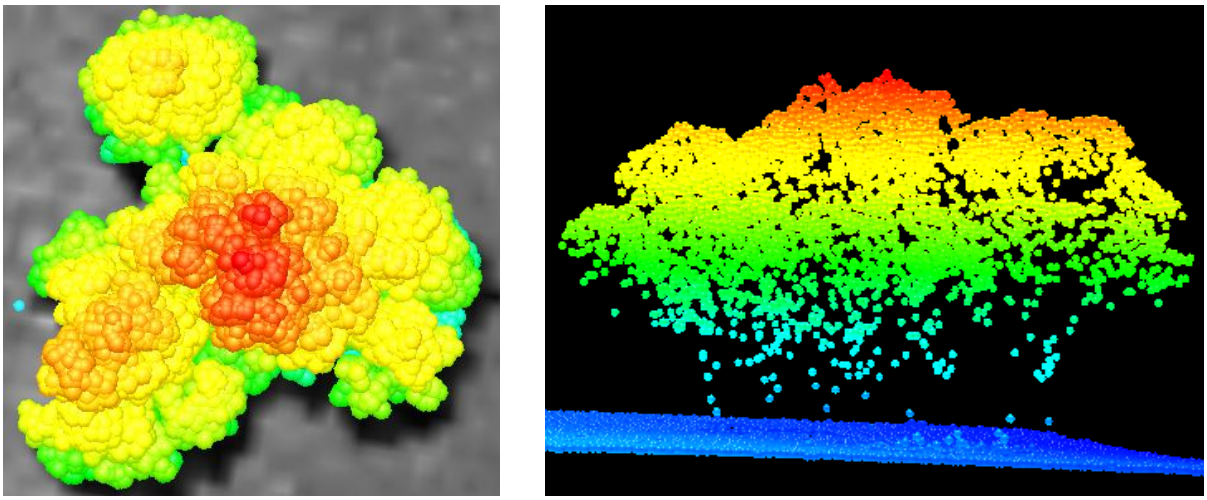

(a) (b)

Figure 8.3: Tree crowns in a cluster as rendered in the FUSION/LDV software. (a) the cluster as seen from above and (b) cross section view of the tree cluster. Cooler colours the trunk and lower part of the crown, while the warmer colours represent the higher end of the crown.

The number of stems in each cluster derived from the three LiDAR based measurements and the actual field measured values are summarised in Table 8.2 and graphed in Figure 8.4. The algorithm with the highest MPE was SAGA GIS (MPE = 4) which consistently underestimated the number of stems in the cluster. In contrast, FUSION exhibited a lower MPE (MPE = 3). It is likely the improved performance resulted from the manual estimation method as it is a one to one method of measurement and the chances of error are very less. The algorithm TreeVaW showed the lowest MPE (MPE = 2). Here the delineation process matched very well with all the candidate clusters except for one location where the number of stems in the cluster was quiet high (15). Nearly 80% (Fig 8.5) of the TreeVaW

results matched the field based results. Although TreeVaW results matched very well with field based results, it was unable to detect smaller trees. This might be the reason for TreeVaW failing in cluster number C7 where most of the trees within the cluster were below 12 m high. SAGA GIS also showed inability in detecting smaller trees as evident from Figure 8.2 (b) where no points were detected over smaller polygons. FUSION method showed a match of nearly 60 % with the field method, whereas SAGA GIS showed a poor performance with only approx 15 % match (Figure 8.5). However, overestimation was observed in C4, where a tree stem was detected in place where actually there is no tree.

Table 8.2. Tree stem number detected by the three algorithms along with the field based measurements.

Cluster ID	Field measured number of stems	FUSION	SAGA GIS	TreeVaW
C1	7	5	3	7
C2	4	3	2	3
C3	3	2	2	3
C4	3	2	1	4
C5	5	2	1	4
C6	3	3	2	3
C7	15	3	2	5

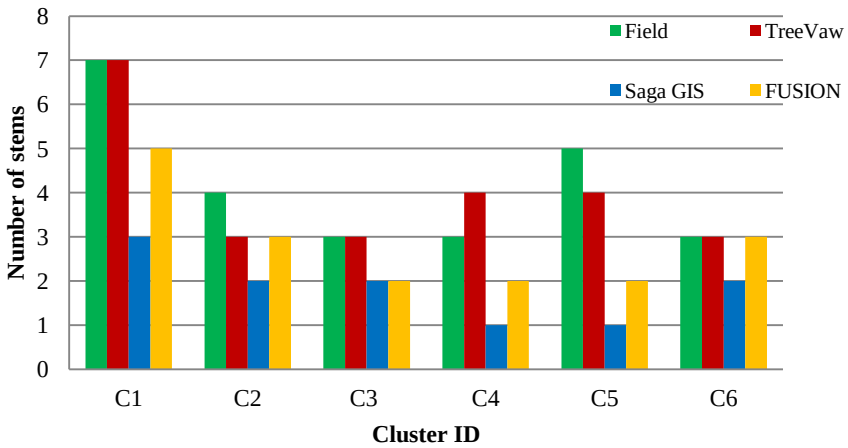

Figure 8.4. Graphical representation of stem numbers as determined by the three different algorithms

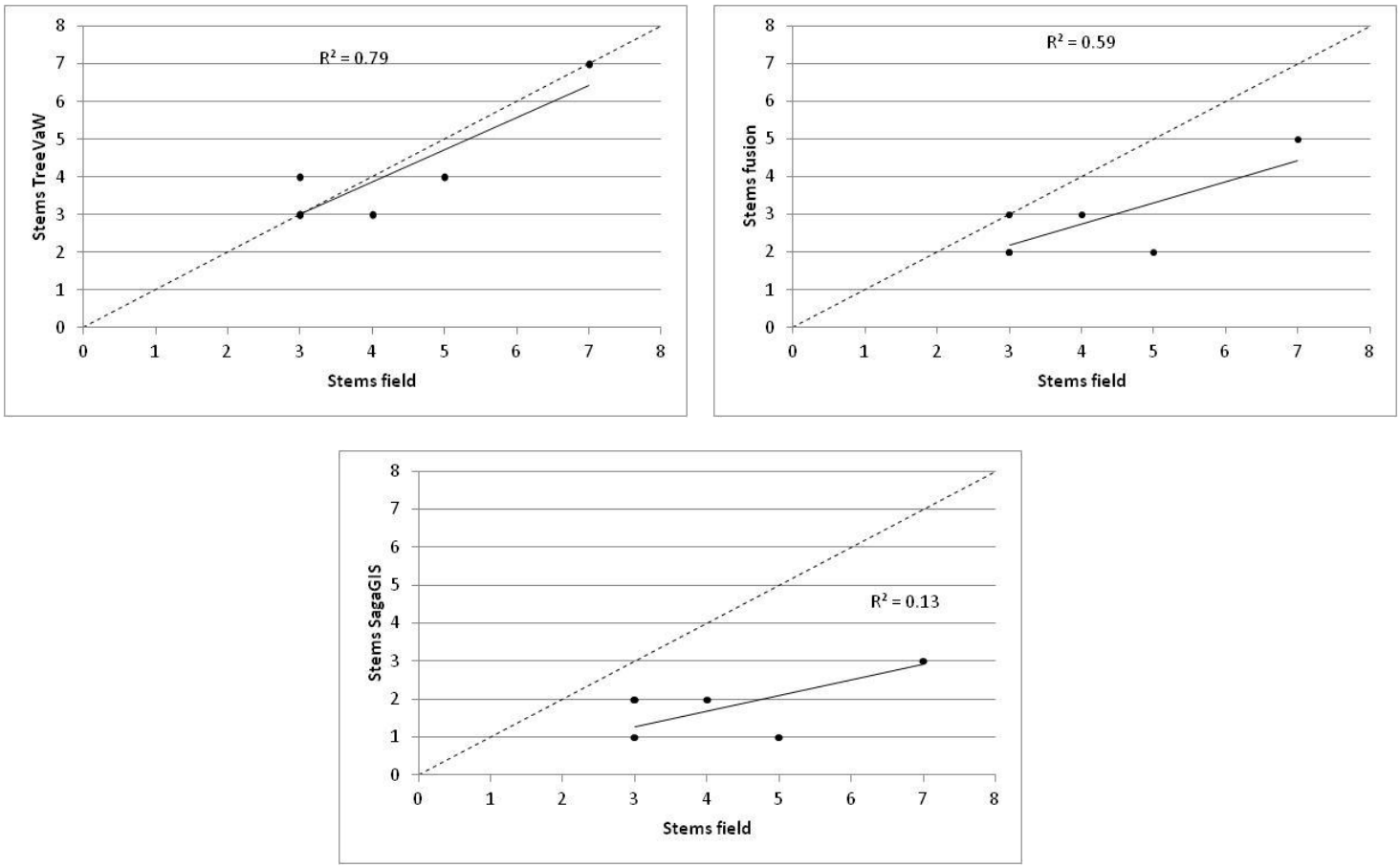

Figure 8.5. Scatter plots of calculated versus actual field measured stem number in the 7 tree clusters. The solid line represents the 1:1 line.

The stem numbers detected in each cluster was later used to estimate the crown area per stem for estimation of average DBH in each cluster. The crown area per stem estimated by the three algorithms is summarized in Table 8.3. TreeVaW estimated average crown area per stem with a MPE of only 12.5 m^2, whereas with FUSION and SAGA GIS resulted in MPE of 42 and 105.5 m^2, respectively.

Table 8.3. The effect on corresponding crown area as per the number of stems detected by three methods.

	Field Based	LiDAR Based		
Cluster ID	CA/Stems (Field)	CA/Stems (TreeVaW)	CA/Stems (SAGA)	CA/Stems (Fusion)
C1	95.84	95.84	223.63	134.18
C2	47.75	63.67	95.50	63.67
C3	117.60	117.60	176.40	176.40
C4	92.50	69.38	277.50	138.75
C5	40.02	50.03	200.10	100.05
C6	80.13	80.13	120.20	80.13
C7	18.66	55.98	139.95	93.30

8.4 Conclusions

The study demonstrated the effectiveness of LiDAR datasets in determining the number of stems in a tree cluster for DBH estimation. The results from three methods were reported namely TreeVaw, SAGA GIS and FUSION in LiDAR data analysis which was satisfactory and supported our hypothesis that remote sensing can exclusively be used for determining tree stems in a cluster. However, there was a difference in estimates between the three algorithms. The discrepancies in number of stems determined from three methods can be due to the complexity in measuring individual trees with LiDAR data and also nature of different algorithms used. The most important factor which may have influenced the tree extraction is the LiDAR pulse striking and reflecting off the tree, and its ability to decipher between the stems. The accuracy is also influenced by other factors like natural terrain conditions including tree canopy, understorey vegetation, small scale topography, and other environmental conditions. However the results were consistent with the findings of other researchers like Edson and Wing (2011).

FUSION is the only process where the trees were detected based on visualization only, and manually identifying a tree which is represented by a three dimensional array of dots (the LiDAR point cloud) (Edson and Wing, 2011), is a difficult task. Differentiating small trees in a cluster was also very difficult and this can be attributed mainly to the LiDAR resolution or the pulse sticking the tree trunk. However, it is a matter of research to determine the optimum pulse rate which would enable the identification of every single resolvable tree in a cluster. TreeVaW and SAGA GIS both rely on a CHM for tree identification and measurement. Hence the accuracy largely depended on the CHM generation. CHM on the other hand is a derivative of DTM and DSM. Hence there is a likelihood of error propagation in the process of CHM generation. SAGA GIS which was based on the concept of watershed segmentation resulted in a poor performance, which can be attributed again to the resolution of the CHM used. TreeVaW algorithm resulted in the best overall performance, and was able to correctly detect trees in the cluster except one cluster where the tree numbers were high (15). However, it appeared to have difficulty finding small trees (<12m). SAGA GIS also was unable to detect smaller trees. Nearly 80% of the trees in the cluster were correctly detected by TreeVaW approach and can be thought to be above other tested algorithms. The high performance of TreeVaW is also because it enables the user to manually incorporate the crown diameter, tree height relationship based on the area and species under consideration.

The prime objective of stem detection was ultimately to apply the results to DBH estimation in tree clusters, which uses canopy area per stem as the predictor variable. An investigation of the effect of these results on relative crown area per stem estimates was carried out, and the results were in accordance with the assumptions that stem numbers would affect the average crown area and in turn DBH estimates. SAGA GIS and FUSION resulted in higher values of average crown area in all the

clusters, which would lead to overestimation of average DBH if these algorithms were to be used. The MPE was highest in case of SAGA (greater than 106 m^2) followed by FUSION algorithm (40 m^2). However, to use the model optimally the number of stem numbers should be possibly very correct, which TreeVaW is able to do with MPE of only 12.5 m^2. Therefore, the study illustrates the effectiveness of LiDAR and TreeVaw algorithm for successfully identifying tree stems in a cluster. We therefore conclude that for DBH estimates in single standing trees optical 2D data is well suited without spending on expensive datasets like LiDAR, however if the aim is to estimate average DBH in a tree clusters the role of LiDAR cannot be ruled out, since LiDAR is considered to be the best source for tree characteristics measurements which are three dimensional in nature.

Chapter 9
Integration of LiDAR and ADS40 imagery for mapping tree species in Australian country "farmscape"

9.1 Introduction

The previous chapters have demonstrated the ability of a number of remote sensing techniques to estimate DBH from tree crown characteristics and even tree height. The ultimate motivation for this work lies in the fact that DBH is the starting point from which estimates of biomass/carbon stocks can be completed (Section 2.1). Identification of tree species is very important in natural resources management and biodiversity studies and, of course, biomass/carbon studies based on allometry rely heavily on species composition as these developed equations are often for specific vegetation types and tree species. The work thus far has indicated that, at least for the 5 eucalyptus species investigated, there is no species dependence on inferring DBH from crown/height parameters of single trees or tree clusters. However this may not be the case for converting DBH to other biomass/carbon related measures, nor can it be assumed that species is not an important covariate when examining the DBH-tree canopy/height relationships for other species.

Similar to other tree characteristics, the conventional means of identifying tree species for forest inventory is through field based methods, which is labor intensive and costly. Scientists have researched in the past to find an alternative means for tree identification, and remote sensing data has been found to provide a valuable source of information on the spatial extent, composition, and structure of species (Ke et al., 2010). Numerous studies have been conducted on species mapping using a variety of remote sensing datasets ranging from multispectral to hyperspectral images (e.g., Vieira et al., 2003; Clark et al. 2005; Goodenough et al., 2003), using multi-temporal data and various spatial resolutions (e.g., Brown de Colstoun et al., 2003; Gerylo et al., 1998), and via multi-sensor image data fusion (e.g., Goodenough et al., 2005).

Ongoing developments in hyperspectral imaging and very high spatial resolution (VHR) image acquisition capability of systems have shifted forest based remote sensing studies from regional-scale (e.g., Wulder et al., 2004) to more detailed forest species mapping at much finer spatial scale. The latter work is relevant in the context of delineating individual tree objects within 'farmscapes'

('farmscapes' having previously being defined in Chapters 3, Verma et al., 2014a; 2014b; Leckie et al., 2003). However, extracting information from high spatial resolution imagery is challenging because of variation in the spectral response of pixels within a target of interest (e.g. trees) (Chapter 3, Verma et al., 2014b; Gougeon and Leckie, 2006; Hirschmugl et al., 2007; Pouliot et al., 2002). Light Detection and Ranging (LiDAR) data (described earlier in Section 7.1) has opened a new avenue for forest species classification in terms of providing 3D information on species-specific vertical crown structure (Gerylo et al., 1998), limb/branch distribution (Dassot et al., 2010b) and even trunk dimensions (Bacher and Mayer., 2000). LiDAR has been used in previous work for individual tree species discrimination (e.g., Brandtberg et al., 2003; Holmgren and Persson, 2004; Liang et al., 2007; Ke et al., 2010). In the process of tree classification, the individual tree crowns are first delineated and then LiDAR-derived metrics for crown structure and shape is used to classify individual trees.
For example, Liang et al. (2007) and Reitberger et al. (2006) distinguished coniferous and deciduous trees with LiDAR data acquired under leaf-off conditions. Here they assumed that, in the leaf-laden coniferous trees, the first and last return pulse signals were reflected essentially only by tree tops while, in deciduous trees, the first return pulse would originate from the tree tops whereas the last return signal would originate from the ground. In this simplistic approach they obtained an overall 89% accuracy in classifying coniferous and deciduous types. In a second study, they used leaf-on data for both species and obtained 80% accuracy for the same classification.

Hollaus et al. (2009) achieved 83% accuracy in discriminating between spruce, larch and beech trees. Their approach used 'geometric information' such as echo width and backscatter cross section as extracted from the full-wave form ALS data to identify the candidate tree species.
Ørka et al. (2007) used two intensity metrics from the return pulses, namely intensity and standard deviation of intensity, to discriminate between birch, European aspen and Norway spruce. They achieved 68% to 74% accuracy in classifying tree species depending on the number of considered variables.

Trees constitute distinct targets; however single tree detection requires high sampling densities. Moreover, individual tree crowns are not always detectable in LiDAR datasets (Persson et al., 2002; Korpela, 2004). Although optical remote sensing (namely satellite and airborne imagery as discussed in previous chapters) and LiDAR data have been used on their own for tree species delineation within forests classification, several studies have sought to combine high resolution multispectral imagery and LiDAR data to produce a 'more effective' species classification within tree communities (e.g., Leckie et al., 2003; Hill and Thomson, 2005; Heinzel et al. (2008); van Ewijk et al., 2014).
Combining the two data types effectively merges the spectral information from the optical imagery, including the objects as derived from OBC discussed earlier in Chapter 3, and the vertical 'structure' attributes of each individual tree from the LiDAR data. Holmgren et al. (2008) integrated LiDAR and

high spatial resolution aerial imagery and obtained 8% improvements in individual-tree-based classification from the combined data. Lidar when used alone resulted in overall accuracy of 88% while Multispectral image for autumn and summer seasons achieved an accuracy of 91% and 84 % respectively. The combined use of the datasets increased the accuracy further by ~5-8%. By combining LiDAR and multispectral autumn images the classification accuracy could be improved to 96%, while combining LiDAR with multispectral summer images could increase the accuracy to only 93%. Their study tested the classification accuracies of two coniferous species; Norway spruce and Scots pine and also deciduous trees. Object based segmentation was first performed which was followed by grouping of points clouds within each segment belonging to each tree. To separate the two species variables like height, canopy shape, proportion of pulse types and intensity of LiDAR returns were derived from the point clouds to capture variations in the crown structure. The relative crown based height helped in separating Scots pine trees with other tree species group.

Heinzel et al. (2008) investigated the use of laser scanning data and CIR (Colour Infra-Red) aerial photographs which were captured simultaneously, for classification of oak, beech and coniferous tree types in Poland. The CIR images were a combination of near infrared, red and green wavebands which were first separated and further transformed into hue, saturation and intensity channels. First 2D single tree delineation was conducted using the algorithm developed by Koch et al (2006). The input data were DSM and DTM which allowed grouping trees in different regions based on the height values. The LiDAR derived polygons were then fitted on the spectral information and the species were classified and crowns were refined. The overall accuracy of classification was 83%.

Machala and Zejdova (2014) mapped the forest species in the region of South Moravia in the Czech Republic using a combination of multispectral image and LiDAR data. Three data sets were used for classification (multispectral image, DEM and DSM). First the vegetation and non vegetation pixels were distinguished using the NDVI layer derived from the multispectral image. Both these broad classes were further classified; the vegetation into forest and non-forest and the non vegetation class into water, clear cut ground and built-up area. A detailed vegetation classification was further performed using a NN classification algorithm followed by a classification based solely on the DEM. The DTM and DSM layers extracted from the LiDAR data were then used in determining the heights of the forest stands, with an overall classification accuracy of more than 80%.

Arroyo et al. (2010) integrated LiDAR and QuickBird imagery for mapping riparian biophysical parameters and land cover types in Australian tropical savannas and obtained an overall accuracy of 85.6%. They first created four different data layers from LiDAR dataset namely DTM (Digital terrain Model, TCM (Tree Canopy Model), PPC (Plant projective cover) and a Streambed map. These layers along with the four-band multispectral image were segmented and classified. Different land cover types were then classified based on four features, namely the mean and standard deviation of both

muti spectral and LiDAR derived information, contextual information such as the relative border to objects classified in a particular class and the NDVI.
Ke et al. (2010) evaluated the 'synergistic use' of high spatial resolution multispectral imagery and low-posting-density LiDAR data for forest species classification in central New York State. They examined three different segmentation and classification schemes namely segmentation based solely on spectral image layers, segmentation based solely on LiDAR derived layers and segmentation based on both spectral and LiDAR derived layers. Object based Image segmentation was performed. Decision tree classification was then used; advantages of such as non parametric in nature and rapid processing, (as discussed earlier in Section 3.3.1) having being identified by the authors. They showed the integration of spectral and LiDAR data improved the species classification compared to using either data source independently. The study revealed that each data source had contributions in species classification. High spatial resolution multispectral imagery helped in defining forest boundaries and provided spectral separation between forest species. LiDAR derived topographic and height information helped in reducing within class spectral variation, enhanced the between class variation due to different height properties among the species and also enhanced the contrast between coniferous and deciduous stands.

As described earlier in Sections 3.1 and 4.1, image classification is the simplest way of extracting information from a remotely sensed imagery, but there are ranges of classification algorithms available which vary from data type, environment and applications. A number of classification algorithms have been developed for both LiDAR and multispectral image datasets, to be used for either type of dataset, or as the previously cited work has shown, to combination datasets. The conventional pixel-based classification method of image classification and information extraction works well with medium to coarse spatial resolution images, but often found to be not sufficient, especially when applied on a very high resolution imagery (e.g., Townshend et al., 2000; Kim and Madden, 2006; Myint et al., 2011) and LiDAR (Ke et al., 2010). When the pixel size of any data layer (LiDAR and image data) is significantly smaller than the average size of the object of interest, object-oriented approach offers an optimal solution for classifying such data (e.g., Kamagata et al., 2006; Verma et al., 2014; Chapter 9) and been successfully applied to forest species classification (Thomas et al., 2003; Wulder and Seemann, 2003).

From the previously cited work above, and given that most of the work to date has focused on delineating vegetation classes, or between broader groups like genus (e.g deciduous from non-deciduous, or pine from Eucalypt) where there are huge differences rather than species. Tree species mapping is obviously a complex task using remote sensing data and challenged by the fact that often not feasible with certain species because of the natural heterogeneity in physical features that often occurs with tree species (Ruiz et al., 2004). Of the reported species classification work using LiDAR

(examples include Holmgren and Persson, 2004; Orka et al., 2009; Brandtberg et al., 2007), the intensity of the backscattered data is commonly used. Several authors have tried to classify tree species using positions of laser points within individual tree crowns as well as the intensity data. (Orka et al., 2009; Holmgren and Persson, 2004). Kim et al. (2009b) reported that by using intensity and the derived height data (from the LiDAR time of flight) improved the classification of deciduous and coniferous species. Kim (2010) classified tree species using cluster analysis and two seasonal LiDAR datasets. The results showed that species with similar tree characteristics seemed to cluster in a single group while the species with different characteristics were clustered in other groups. They concluded that the use of two season datasets led to more reasonable clusters than using either one of the datasets. In the work of Ke et al. (2010) mentioned earlier, the DSM and height data from LiDAR helped in classifying elevation specific stands like Hemlock. They concluded that the LiDAR derived topographic features increased the classification accuracy by reducing the within class variation among the neighbouring objects caused by shadow effects.

So, while optical data has proven useful in forestry applications for differentiating between forest and non-forest areas (Lehmann et al., 2011), where there is generally a considerable difference in tree morphology, and for discriminating between major tree species within a forest, such as coniferous and deciduous (Chastain and Townsend, 2007), they cannot detect features underneath areas of dense canopy top-cover nor do they provide information on the vertical composition of vegetation-related attributes. LiDAR data, on the other hand, allow analysts to directly portray forests in a three-dimensional format over large areas, however, the data have their own shortcomings. LiDAR data provide multiple return position and intensity measurements, but contain only limited information for deriving the correspondence to target objects. A review of the rapidly growing literature on LiDAR applications emphasizes the need for optical data fusion with LiDAR data to improve various feature extraction tasks (Hill and Thompson, 2005; Leckie et al., 2003).

The objective of this chapter therefore, is to investigate whether the same approach of fusing multispectral images and LiDAR data allows us to classify the constituent Eucalyptus species that make up the scattered trees in our ‘farmscape’. In this chapter we will separately use the LiDAR and high resolution multispectral images as well as a combination of the two.

9.2 Materials and Methods

9.2.1 Study Area

The study area used in this work is the same as that described earlier in Chapter 5 (Section 5.3.1), mix of forested area (Mount Duval), open woodland and mixed pastures. Much of the farm area is dominated by 5 Eucalypt species of varying age and stem and canopy density. The major species

occurring in the area are Apple Box (AB, *Eucalyptus bridgesiana*) Stringy Bark (SB, *Eucalyptus caliginosa*), Red Gum (RG, *Eucalyptus blakelyi*), White Gum (WG, *Eucalyptus viminalis*), and Yellow Box (YB, *Eucalyptus melliodora*). A total of 88 trees comprising these 5 species (SB-34, WG-18, YB-31, AB-15 and RG-5) were used for the training and validation process.

9.2.2 Remote sensing datasets

Multispectral imagery of the study area was acquired at approximately 1045 hrs (AEST) on 3 November 2011 using an ADS40 airborne digital scanner described earlier in Chapter 5 (Section 5.3.2). Flown at an altitude of 1920 m above ground level (AGL), the 24-bit images were acquired with a spatial resolution of approximately 50 cm in five spectral bands: Band 1 (NIR 0.7-1 μm), Band 2 (Red 0.6-0.7 μm), and Band 3 (Green 0.5-0.6 μm), Band 4 (Blue 0.4-0.5 μm). The image transects were mosaiced and the complete image geo-referenced using ground control (Section 5.3.2).

The LiDAR data, previously described in Section 7.2.3, was acquired on June 1, 2013 using a Trimble Harrier 68i/G1 system. The LiDAR data encompassed an area of approximately 200 ha (previously described in Section 7.2.3), which included the 5 Eucalyptus species. Using the raw point dataset, a DTM was created from the last return data, a digital surface model (DSM) from the first return data and, by subtracting the DTM from the DSM, a canopy Height Model (CHM) with a vertical resolution of 1m was also created.

9.3 Methodology

Object based segmentation and classification can be grouped broadly as a three step process. 1) Segmentation which is grouping of features called objects. 2) Defining the object based metrics and 3) Classification based on these defined metrics. This study investigated each of these steps to improve forest species classification through integration of multispectral ADS40 imagery and 3-dimensional LiDAR data. eCognition Developer 8.64 software (formerly Definiens) of Trimble Germany GmbH (München, Germany), which was specifically created as a powerful instrument for object-oriented image analysis (Benz et al., 2004), was chosen for the purposes of this study.

9.3.1 Image Segmentation and Classification

Image segmentation was carried out on three different image types: (1) the individual bands of the ADS40 (spectral-based); (2) LiDAR derived layers (LiDAR-based); and (3) both the spectral and LiDAR derived layers (Spectral/LiDAR based). For the image segmentation process, the spectral and shape homogeneity criterion based on color/shape ratio, compactness/smoothness ratio for object shape, and a scale parameter for resultant object size and the input layer weighting were stipulated. Since the three segmentation processes, namely that applied to the multispectral data only, the LiDAR

data only, and spectral/LiDAR-combination, were different in their characteristics, hence the user specified parameter settings varied between the data types. Here the optimum parameter values were determined by trial and error, with a visual assessment of the final canopy boundaries used to assess the veracity of the settings. The image layer weights were tailored for the best differentiation of tree/cluster areas, with greater weights assigned to the green and NIR bands (e.g., Gitelson et al., 1996). For LiDAR-based segmentation, the three layers namely height (return differences), CHM and intensity were used. Higher weights were assigned to CHM and height and the lowest weight to the intensity image as the characteristics of the intensity image depends on various environmental factors (e.g., Im et al., 2008). In the case of the spectral/LiDAR based segmentation involving a combination of the above two datasets, the same weighting was applied to the collective image and LiDAR datasets, respectively. Table 9.1 summarizes the values assigned to each parameter in each scheme. Though segmentation largely depends on the scale parameter, as it affects the granularity of the objects formed Chapter 3 (Section 3.3.1), changing the shape and compactness also led to an increase in the quality of segmentation results, as observed, for example in Machala and Zejdova (2014). A range of segmentation with different scale parameters were carried out and tested before reaching to the optimal scale for each dataset.

A number of object based metrics were calculated based on the spectral, the topographic (ie CHM, DTM, DSM) and the intensity information. Together with mean and standard deviation of segmentation layers, higher-order texture measurements such as GLCM (Grey Level Co-occurrence Matrix) and GLDV (Grey-Level Difference Vector) (Haralick, 1986) were derived for the green and near infrared bands because of their usefulness in species discrimination (e.g., Gitelson et al., 1996). Other geometric metrics of objects (e.g., shape etc.) were not computed as they are generally not found useful in vegetation classification (e.g., Yu et al., 2006). Overall, a total of 26 metrics were generated, 20 metrics derived from ADS40 multispectral layers, 6 from the LiDAR-derived topographic layers (Table 9.1).

Spectral features such as mean, brightness and standard deviation of the spectral bands were calculated using the segmentation bands. Spectral indices like normalized difference vegetation index (NDVI) and the simple ratio (SR) were calculated using Red and IR bands, as was the area of each segmented region and its relationship to neighboring objects. Statistically significant features were then tested with the feature space optimization tool within eCognition. When defining the feature space, some textural features were also tested (Textures after Haralick - GLCM Mean, Standard Deviation, Homogeneity and Contrast).

Table 9.1 : Metrics defined for rule based classification

Datasets	Data Layers	Object Metrics
Multispectral ADS40	Blue	Mean and standard deviation of each layers
	Green	Brightness of each layer
	Red	GLCM mean and standard deviation for green and IR
	Infra Red	GLDV mean and contrast for green and IR
LiDAR	CHM	Mean and standard deviation of each layer
	Height	
	Intensity	

Rule-based classification was used in this study for classification of segmented objects into five different Eucalypt tree species, namely Stringy Bark (SB), White Gum (WG), Yellow Box (YB), Apple Box (AB) and Red Gum (RG). Training point features for each of the species were collected from each of the data types (ie image only, LiDAR only or integrated image-LiDAR) and used to classify the respective segmented objects. The approach for classifying individual tree species was to define rules based upon metrics best describing the training features. Classification of the LiDAR data was based on seven tree height ranges, namely 5-10 m, 10-15 m, 15-20 m, 20-25 m, 25-30 m, 30-35 m, 35-40 m and > 40 m, based on the nature of the species observed in the field. Based on the intensity values and height, trees were classified in five different categories, taking reference from the field based measurements. The classification of multispectral ADS40 which can be thought of as a combination of supervised and unsupervised classification approach where the rules were able to detect the species class which was later given a specific species name with the help from field based measurements.

9.3.2 Accuracy Assessment

Field sampling was conducted in the month of September through December 2012. Field measurements of vegetation structural properties along with species information were collected during this period. Depending upon tree species available in the study area, all 88 samples pertaining to the five different Eucalypt types (SB-34, WG-18, YB-31, AB-15 and RG-5) were used to assess the classification accuracy. The field based tree locations were converted into point coverage along with the tree attributes using ARCGIS ver. 10. These field sampling locations which represented the sample size for each class was used to evaluate the accuracy with which the trees have been classified. An error matrix was constructed to estimate the classification accuracy which consisted of producer's

accuracy (PA), user's accuracy (UA), overall accuracy and Kappa co-efficient. The error matrix was generated for all the three classification results and was compared. Comparisons between Kappa coefficients were performed to evaluate the effect of (1) the integration of spectral data and LiDAR data in image segmentation, (2) the integration of spectral and LiDAR data sources in classification.

9.4 Results and Discussion

An example of coincident LiDAR and multispectral image data (without radiometric scales) for a small subset of the overall study area is given in Figure 9.1.

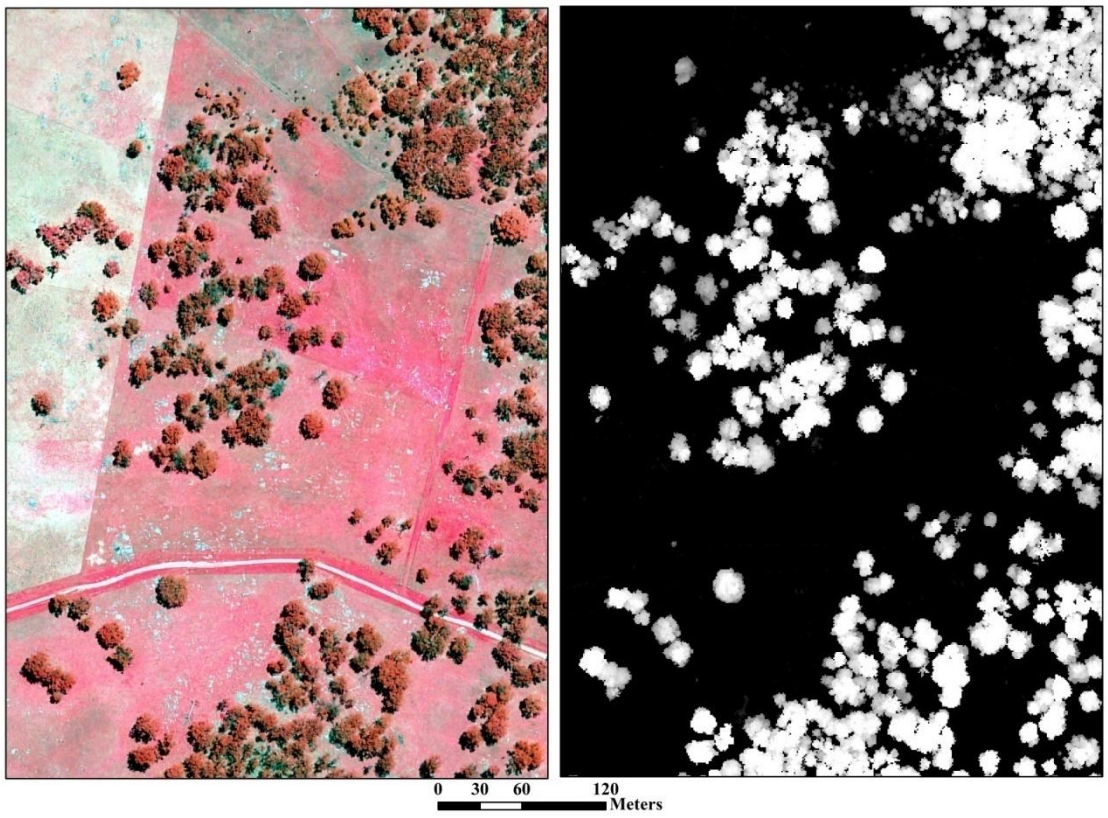

Figure 9.1 (a) ADS40 multispectral image of the study area rendered in false colour, and (b) grey-scale CHM of 1m vertical resolution derived from the LiDAR returns (no radiometric scale for brevity)

As expected, a visual examination the objects generated from the various segmentation processes showed the outputs to be highly dependent on the scale parameters (Table 9.2).

Table 9.2 : Applied data segmentation parameters

Datasets	Data Layers	Weight assigned	Scale	Color and Shape parameter	Compactness smoothness
Multispectral ADS40	Blue	1	70	0.2	0.5
	Green	5			
	Red	1			
	Infra Red	5			
LiDAR	CHM	5	70	0.7	0.5
	Height	5			
	Intensity	0.5			
LiDAR/Multispectral ADS40 combined	CHM	2	270	0.7	0.9
	Height	5			
	Intensity	0.5			
	Blue	1			
	Green	5			
	Red	1			
	Infra Red	5			

A Scale of 70 was found to be effective in delineating tree crowns in the LiDAR and multispectral data datasets (Figure 9.2(a) and 9(b)) whereas a larger Scale value (270) worked very well with the combined multispectral/LiDAR data, effectively delineating the tree crowns (Figure 9.2(c)). A close look at the segmentation results of the LiDAR CHM showed elongated segments (Figure 9.2(b)) but only on the low value (of CHM) areas. This is expected given the vertical resolution of the derived CHM, when there is low understory and the ground surface is relatively heterogeneous. However, this did not affect the delineation of tree crowns given their considerable heights (~ 10 m) above the ground surface. The segmentation process was more challenged for the multispectral image data; segmentation at lower scale values appeared fragmented while larger values of Scale resulted in more generalization with some of the understory cover found included within the crown segment (as encountered and discussed earlier in Chapter 3, (Section 3.3.1). However, this could have been overcome by the use of stepwise segmentation, but did not try here. In addition to the value of Scale,

the relative weights assigned to the image layer, the color/shape ratios and smoothness/compactness ratios also had an influence on segmentation.

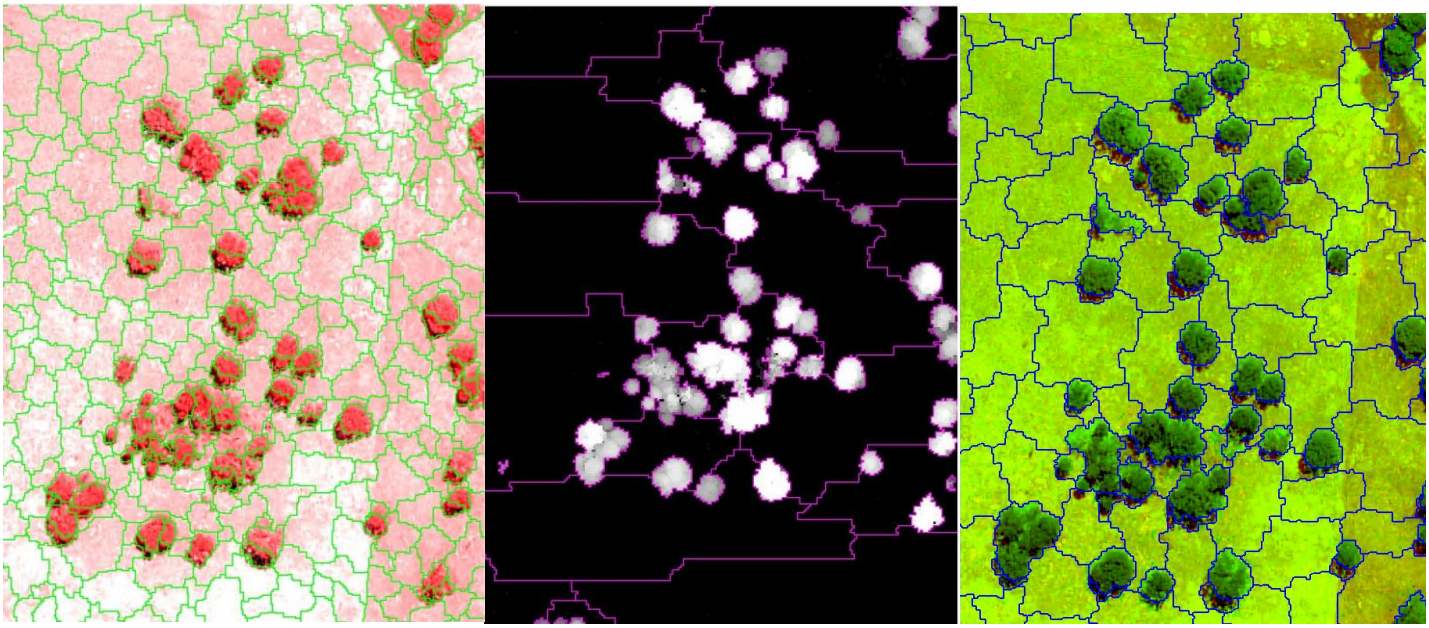

Figure 9.2 Examples of the result of data segmentation (a) ADS40 multispectral image (b) 1 m resolution CHM derived from the LiDAR data, and (c) combined LiDAR/multispectral data.

The confusion matrix summarizing the classification performance of the three datasets is given in Table 9.3. A classification based on the combined use of LiDAR and multispectral imagery yielded the highest classification accuracy with an overall accuracy of 60.5%. Unlike the multispectral imagery, the shadows were well segmented from the canopy envelopes in the combined datasets, owing to the LiDAR derived height information.

The lowest accuracy achieved by the multispectral data layers echoes previously identified challenges (Section 3.3.1) that spectral metrics such as mean and brightness did help in delineating tree crown from exposed understory and while the textural properties helped in separating species, these metrics were found not very effective in discriminating between the crown envelop and understory vegetation. The NDVI layer did not significantly improve the image-based segmentation.

The species Red Gum and Apple Box were the most difficult to classify using the multispectral dataset due to their occurrence in lesser numbers in the study area. Stringy bark was found to coexist with the Apple Box and to a lesser extent the White Gum, while Red Gum the least accurately classified was mixed in all of the other categories. The highest classification accuracy achieved, based on spectral and texture metrics, was for the Stringy bark species.

Table 9.3 Comparison of species classification accuracy (%)

	Multispectral		**LiDAR**		**Combined**	
Species Name	PA	UA	PA	UA	PA	UA
Yellow box	39.02	64.42	61.44	66.73	63.93	76.14
Stringy Bark	74.84	40.15	62.19	32.88	74.9	43.54
White Gum	32.25	49.92	42.16	82.91	42.95	93.21
Red Gum	21.28	5.48	89.1	28.49	73.76	42.04
Apple Box	2.75	5.33	39.06	26.62	60.54	50.29
Overall Accuracy	39.06%		48.56%		60.99%	
Kappa	0.22		0.43		0.51	

PA = producer's accuracy, UA = user's accuracy

Clearly the ancillary LiDAR derived layers helped in classifying trees based on different height ranges. However, when species-wise classification was performed using these height ranges only, a substantial amount of intermixing was observed especially between String Bark and White Gum. It was however easier to classify species like Apple Box and Red gum as they behaved differently so far as tree height and tree structure is concerned. The topographic information helped in increasing the classification accuracy, but intensity data did not contribute much and therefore the classification rely only on height information in this case. A preliminary classification results based on seven different height ranges were found satisfactory with respect to field based measurements. This helped in identifying species that can be classified on the basis of height ranges. The following observations were made with respect to height based classification: (a) White gum was classified well because of its huge crown and tree height characteristics; (b) the same logic can be applied for Apple Box due to its typical height characteristics, however, a substantial amount of intermixing of Apple Box with other species was observed throughout the study area and hence height information alone is not working very well in this case; (c) trees with intermingled crowns were difficult to classify and edge of the tree crown were misclassified in all case; (d) Yellow Box and Stringy bark showed maximum mixing probably due to overlapping height ranges. To overcome this, tree crown area were taken into consideration which helped in refining the accuracy as Yellow Box had larger crown compared to Stringy bark. The confusion in case of tree edges could be due to LiDAR returns. Figure 9.3 shows an example of the height based classification results.

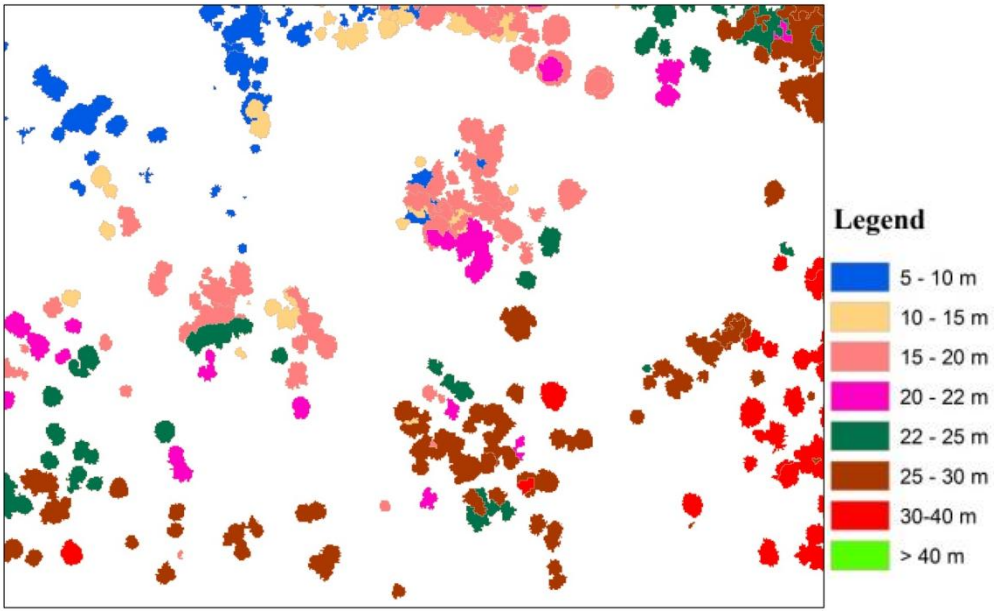

Figure 9.3 Classification output based on height ranges of LiDAR

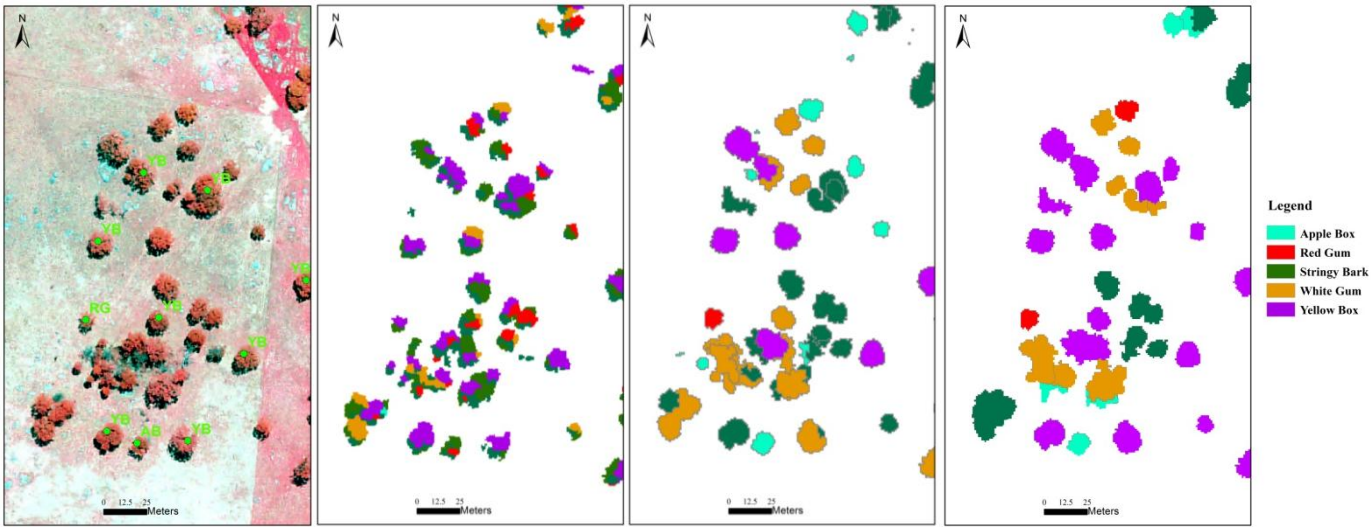

Figure 9.4 The species classifications generated using (a) ADS40 multispectral image, (b) 1 m resolution CHM derived from the LiDAR data, and (c) the combined LiDAR/multispectral datasets.

The combined use of LiDAR and multispectral data allowed accurate identification of tree species with the overall classification accuracy of 61 % (kappa 0.51) at scale 270. The inclusion of 'topographic' attributes along with (image) spectral information in the classification increasing the overall classification accuracy by ~ 20 %. Similar findings were reported by others (e.g., Ke at al., 2010). Fig 9.4 shows the classified outputs for all the three datasets. Apple Box compared to all other

tree species performed better in LiDAR and good with the combined use of the two. Stringy bark was classified well by the single and combined use of the datasets firstly due to abundance and secondly due to a distinct crown shape.

9.5 Conclusions

The study evaluated the accuracy of classifying 5 different species of Eucalypt trees scattered (individually and in small clusters) across a farmscape using LiDAR and multispectral imagery (ADS40), both individually and in combination. The spectral based classification approach using multispectral data; a mix of supervised and unsupervised classification system, proved unable to differentiate between the species because of the heterogeneity associated with the image. Of the 4 wavebands available in the image, the green and infrared bands helped the most. The relatively poor classification accuracy (39.06 %) of the segmentation suggests that a multi-level hierarchical classification approach would more likely increase the accuracy and overcome the heterogeneity (Ke at al., 2010).

The height based discrimination available to the LiDAR data, while only slightly improving the classification accuracy compared to the image-based dataset, illustrated the limitations of relying only on height groupings as a means of discriminating tree species, especially when single tree (and even small clusters) is not growth limited due to competition. Other metrics like tree canopy shape, spectral information within the tree crown, the intensity of laser returns and type of laser returns could also be taken into account for tree species discrimination, similar to the study carried by Holmgren et al, 2008. However, this is a matter of further research. The overall accuracy (48.56 %) achieved was higher by around 10 % than the multispectral alone. The classification accuracy largely depends on the accuracy of the segmentation achieved. The contrast associated with the LiDAR dataset helped in achieving better segmentation results than multispectral.

The integration of LiDAR and multispectral data resulted in more accurate species classification than using either of the dataset independently. The inclusion of height information helped overcome at places where the spectral and textural attributes failed resulting in higher overall accuracy (60.5 %).

Chapter 10
Conclusions

10.1 Summary

Image-based remote sensing systems have evolved rapidly with metre resolution satellite systems such as WorldView2, and sub-metre airborne systems now widely available. The main objective of this thesis was to investigate the potential of very high resolution, image-based remote sensing data for estimating a key parameter, namely the diameter at breast height (DBH) of scattered Eucalyptus trees in typical grazing farmland in south eastern Australia. Whilst more sophisticated airborne scanning techniques such as LiDAR are gaining prominence for their ability to provide detailed surface and structural measurements of tree canopies, imaging systems are currently simpler to deploy and operate, and the data, per unit area of acquisition remain (at least to date) considerably cheaper to acquire. There are however attributes of trees that only LiDAR is capable of directly measuring, such as vertical canopy dimensions and porosity. Consequently LiDAR data have also featured in this work as an adjunct to the image datasets; the integration of which was used in delineating, for example the individual species of Eucalyptus that featured in this work.

Owing to the importance of Eucalypt species in an Australian landscape, and in particularly in the New England region of south eastern Australia where this work was conducted, five different species; *Eucalyptus bridgesiana, Eucalyptus caliginosa, Eucalyptus blakelyi, Eucalyptus viminalis, and Eucalyptus melliodora* of genus eucalyptus were studied. Simple regression models were developed linking the crown projection area and height of both isolated trees and for tree clusters of up to 27 stems, to DBH. Based solely on ground measurements, the model explained 67% and 68%, respectively, of the variance in stem DBH in two cases. A single model involving both single trees and the tree clusters to predict average stem DBH had similar explanatory power ($R^2 = 0.71$) and yielded a mean prediction error in average DBH per stem of ±13 cm. The results also indicated that it was sufficient to use crown projection area for DBH prediction, however, it was found that the inclusion of tree height as a parameter in the equations increased, slightly, the overall accuracy of DBH estimations. The results of this study established the fact that DBH of the scattered Eucalyptus trees could be estimated using crown projection area, which itself is a measured variable from remote sensing data. Very high spatial resolution (15 cm) aerial imagery, and high spatial resolution (50 cm) airborne (Airborne Digital Sensor, ADS40), and satellite (World View 2, WV2) imagery were then evaluated for their use in identificating and delineating tree canopies, from which crown projection area and crown diameter could subsequently be extracted. Owing to the complexity of high resolution

remote sensing data both pixel based and object based image classification schemes were tested with a very high spatial resolution CIR image (15 cm). This study served to highlight the advantages and disadvanteges associated with pixel and object based image classification, and in the latter, the important role played by setting the appropriate feature parameters in delineating the desired objects (ie tree crowns). The results verified that the object-based classification of individual tree crowns (or crown clusters) had an improvement in overall classification accuracy compared to the pixel-based classification, . In addition to this, an attempt was also made to quantify the variation in tree cover area estimates taking manual method of vectorization as a reference. For this study WV2 data set with a spatial resolution of 50 cm was used. This study showed that both the object based and supervised pixel-based method of classification performed equally well and that the spatial resolution, within the range of this work, did not overly effect the accuracy of tree area estimations. This research explored the potential of using remote sensing data of tree crowns as a possible alternative for field based measurements for estimating the diameter at breast height (DBH). Considering the limitations associated with airborne images in terms of their availability, temporal resolution and the often significant image acquisition costs, an attempt was made to replace airborne image data with that from space borne platforms of similar spatial resolution. The relative performance of three sensors in terms of crown area extraction was investigated to determinate an appropriate spatial resolution of image datasets necessary to extract tree crown descriptors in scattered trees and tree clusters in a typical farmscape. The remote sensing data: ADS40 digital airborne imaging (50 cm), spaceborne WorldView2 (50 cm) and Color Infrared (CIR) imagery (15 cm) were tested for their ability to infer crown characteristics. \

Even though crown projection area proved to be the most accurate parameter from which to infer DBH, the results also indicated that inclusion of a tree height measurement could increase the predictive performance. A shadow-based method for estimating the height of single eucalyptus trees from the very high spatial resolution imagery was proposed and tested. The method used the projected tree shadows on the ground, taking into account ground slope and aspect and solar illumination angles (elevation and azimuth). The accuracy of the height estimated in this work (MPE/RMSE ±5.6 m) demonstrated a possible pathway to inferring the height of individual trees from imagery alone.

Possibly the least expected of the results in this work was the fact that the canopy projected area-DBH relationship for single eucalyptus trees (of 5 species) and the average canopy projected area-average DBH relationship for tree clusters containing between 2 and 25 stems, were statistically indistinguishable. Although high resolution remote sensing data was found useful in extracting projected crown dimensions for tree clusters, from which the average DBH within the cluster can be derived, calculating the total DBH within the cluster requires knowledge of the number of stems within the cluster. This study explored the utility of LiDAR data to estimate tree height of single trees

and also to ascertain stem numbers within a tree cluster. The LiDAR based measurement method estimated tree height with a MPE of 1.44 m (6.5 % error). Similarly LiDAR based stem density measurements were in agreement with the field based measurements. The results led to the conclusion that the algorithm TreeVaw came up with the best estimate with MPE of 2 trees; the downside being that TreeVaw failed with smaller trees which were less than 12m high.

The data also helped in quantifying canopy volume of our candidate eucalypts, an important factor in inferring tree yield, with achieved estimation accuracies very close to the field based measurements. Both the image and LiDAR datasets were also combined in an attempt to delineate the individual Eucalyptus species within the area of study. Here the image and LiDAR datasets were used separately and also in combination to assess their ability in generating species descriptions for this study. The combined image-LiDAR datasets proved most effective in delineating between the species.

Overall, the study suggests that even though both LiDAR and multispectral imagery could effectively be used to estimate tree characteristic estimates like tree height, canopy dimensions, canopy volume, species, LiDAR achieved better estimation accuracies than multispectral datasets. However owing to the cost associated with the LiDAR datasets, it would not be thought to be fit for larger areas in terms of cost and time.

Overall, the research demonstrated the potential of using image-based methods for estimating DBH in our candidate trees and tree clusters with an accuracy that may equal that of the significantly more expensive and complex LiDAR systems. As with other technologies, the cost of LiDAR systems and data acquisition will likely decrease in time and such data will become more widely available. The research demonstrated the potential of using image-based remote sensing data as a plausible alternative not only for field based measurements of DBH and other tree parameters estimations at farmscape level studies, but as an alternative to LiDAR-type systems. However, where 3D tree descriptors are necessary, for example to quantify canopy volume, overall tree biomassand possibly for tree species identification, LiDAR along with image data are an effective combination. In other words, remotely sensed imagery for DBH and biomass assessment in scattered trees and tree clusters in farmscapes will continue to play an important role in the future .

10.2 Scope for further work

The study developed and applied a combination of field and remote sensing based tree measurements to five different Eucalyptus species in north eastern New South Wales, Australia. Such allomteric models are often site and species specific; hence the performance of these models needs to be tested for Eucalyptus species in other regions as well. While encouraging as the cluster versus single tree

model comparison was, it is of considerable interest to test this assertion, again over a larger range of species and in different regions.

Of course, the landscape investigated in this work was only 662 ha, and while encapsulating considerable variation in soils, elevation and aspect (for example as reported in Garraway and Lamb, 2011), it would be expected that the robustness and precision of any model could potentially be enhanced by including other landscape parameters. While this study was supported by sophisticated remote sensing datasets like LiDAR, which offers the advantage of large area coverage, the cost of acquiring the LiDAR data restricted the analysis to a very small area for the stem density study with few sample points and this means the results are less likely to be applicable to other areas. Terrestrial scanning system which has widely been used in Australia could also seem as an alternative, as these provide data in much finer details. Airborne laser scanning provides digital terrain model at 10-50 cm precision digital height model at about 1m precision (Mass 2005), whereas terrestrial laser scanning provides data with precise stem geometry information which can be relied upon.

Remote sensing and conventional field based methods have been extensively used in forest based studies but not so in farmscapes which contain scattered trees. Our native eucalyptus trees, both individual and in clusters are an important feature of our farmscapes and they contribute significantly to above and below-ground carbon stocks in these landscapes. There will be a growing need to assess carbon and biomass stocks across our farmscapes in order to fully quantify carbon storage change in response to management and provide evidence-based support for carbon inventory and ultimately carbon trading. Such large scale assessments are likely to only ever be feasible using remote sensing techniques.

The method for tree crown identification undertaken in the above study was Object based image classification using k-NN technique. As an initiation to further research the author would like to test other non parametric classification techniques like SVM and Decision tree and their performance in forest landscape. It is also a matter of further research to have an insight into other tree metrics like percentage plan cover, crown porosity and percentage foliage cover, which have not been undertaken in the present research.

References

Agresti, A., 1996. *An Introduction to Categorical Data Analysis*, Wiley, New York, 312 p.

Albrigo, L. G., C. A. Anderson, and G. J. Edwards. 1975. Yield estimation of 'Valencia' orange research plots and groves. *Proc. Fla. State Hort. Soc.* 88: 44–49

Andersen, H. 2009. Using airborne light detection and ranging (LIDAR) to characterize forest stand condition on the Kenai peninsula of Alaska. *Western Journal of Applied Forestry*. 24, 95–102.

Apan A.A. (1997). Land cover mapping for tropical forest rehabilitation planning using remotely-sensed data. *International Journal of Remote Sensing*, 18(5): 1029–1049.

Aplin, P., P. Atkinson, P.Curran, 1997. Fine spatial resolution satellite sensors for the next decade. *International Journal of Remote Sensing* 18, 3873–3881.

Arzai, A.H., Aliyu, B.S., 2010. The relationship between canopy width, height and trunk size in some tree species growing in the savana zone of Nigeria. *Bajopas*. 3(1), 260–263

Asner, G.P., Palace, M., Keller, M., Pereira Jr., R., Silva, J.N. M. and Zweede, J.C. (2002). Estimating canopy structure in an Amazon forest from laser range finder and IKONOS satellite observations. *Biotropica*, 34(4): 483–492.

Asner, G.P., and Warner, A.S., 2003. Canopy shadow in IKONOS satellite observations of tropical forests and savannas. *Remote Sensing of Environ*ment, 87(4): 521–533, doi:10.1016/j.rse.2003.08.006

Attiwill, P.M., Adams, M.A., (Eds) 1996. *Nutrition of Eucalypts (CSIRO Publishing)* 448 pages.

Baatz, M. and A. Schape, 2000, Multiresolution segmentation—an optimization approach for high quality multi-scale image segmentation. In Angewandte Geographische Informationsverarbeitung XII, Beitra¨ge zum AGIT-*Symposium Salzburg 2000* (Karlsruhe: Herbert Wichmann Verlag), pp. 12–23.

Baatz, M., U. Benz, S. Dehghani, M. Heynen, A. H¨ oltje, P. Hofmann, I. Lingenfelder, *et al.* 2004. *eCognition professional user guide, version 4.0. Definiens Imaging GmbH*. Munchen, Germany: Definiens.

Bacher, U., & Mayer, H. (2000). Automatic extraction of trees in urban areas from aerial imagery. *International Archives of Photogrammetry and Remote Sensing*, 33(Part B 3/1), 51 – 57.

Baffetta, F., Corona, P., Fattorini, L., 2011. Assessing the attributes of scattered trees outside the forest by a multi-phase sampling strategy. *Forest.* 84 (3), 315–325

Barbosa, P.M., Stroppiana, D., Grégoire, J.M., Pereira, J.M.C., 1999. An assessment of vegetation fire in Africa (1981–1991): Burned areas, burned biomass, and atmospheric emissions. Global Biogeochemical Cycles 13, 933-950.

Barnes, P., Wilson, B.R., Trotter, M.G., Lamb, D.W., Reid, N., Koen, T., 2011a. The patterns of grazed pasture associated with scattered trees across an Australian temperate landscape: an investigation of pasture quantity and quality. *Rangel. J.* 33, 121–130.

Barnes, P., Wilson, B.R., Reid, N., Koen, T.B., Lockwood, P., Lamb, D.W., 2011b. Litterfall and associated nutrient pools extend beyond the canopy of scattered eucalypt trees in temperate pastures. *Plant Soil*. 345, 339–352

Beets, P.N., Kimberley, M.O., Oliver, G.R., Pearce, S.H., Graham, J.D., Brandon, A., 2012. Allometric Equations for Estimating Carbon Stocks in Natural Forest in New Zealand. *Forests*. 3, 818–839.

Bella, I.E., 1971. A new competition model for individual trees. *Forest. Science*. 17, 364–372

Benz, U. C., P., Hoffmann, G., Willhauck, I., Lingenfelder, and M., Heynen, 2004. Multi-resolution Object-oriented Fuzzy analysis of Remote Sensing Data for GIS-ready Information. *ISPRS Journal of Photogrammetry and Remote Sensing*, 58, pp. 239–258.

Benediktsson, J.A., Pesaresi, M. and Arnason, K. (2003). Classification and feature extraction for remote sensing images from urban areas based on morphological transformations. *IEEE Transactions on Geoscience and Remote Sensing*, 41 (9): 1940–1949.

Bertolette, D. R., & Spotskey, D. B (1999). Fuel model and forest type mapping for FARSITE input. In G. E. Gollberg (Ed.), *The joint fire science conference and workshop*. Boise, ID: University of Idaho and International Association of Wildland Fire.

Bergen, K., Colwell, J. and Sapio, F. "Remote sensing and forestry: Collaborative implementation for a new century of forest information solutions", *Journal of Forestry*, vol. 98, no. 6, pp. 4–9, 2000

Biging, G.S., Dobbertin, M., 1992. A Comparison of Distance-Dependent Competition Measures for Height and Basal Area Growth of Individual Conifer Trees. *Forest Science*. 38(3), 695–720.

Biging, G.S., Dobbertin, M., 1995. Evaluation of Competition Indices in Individual Tree Growth Models. *Forest Science*. 41 (2), 360–377.

Bird, P., Bicknell, D., Bulman, P., Burke, S., Leys, J., Parker, J., 1992. The role of shelter in Australia for protecting soils, plants and livestock. *Agroforest. Sys*. 20, 59–86.

Blaschke, T., 2010. Object based image analysis for remote sensing. *ISPRS Journal of Photogrammetry and Remote Sensing*, **65**(1): 2–16.

Blaschke, T., and J. Strobl, 2001. What's wrong with pixels? Some recent developments interfacing remote sensing and GIS. *GeoBIT/GIS*, **6**: 12–17.

BoM., 2014. Bureau of Meteorology Climate Statistics for Australian Locations: Armidale airport. http://www.bom.gov.au/climate/averages/tables/cw_056238.shtml. *Accessed 3rd March 2014*.

Brambley, R.G.V., P.A. Hill, P.J. Thorburn, F.J. Kroon, and K. Panten., 2008. Precision Agriculture for improved environmental outcomes: Some Australian perspectives. *Landbauforschung*. 58:161–178.

Brandtberg, T., Warner, T., Landenberg, R., & McGraw, J. (2003). Detection and analysis of individual leaf-off tree crowns in small footprint, high sampling density lidar data from the eastern deciduous forest in North America. *Remote Sensing of Environment*,85, 290−303.

Breiman, L., J. Friedman, R. Olshen, and C.J. Stone, 1984. *Classification and Regression Trees*, Chapman and Hall, New York, 146–150 p

Brieman, L. 2001. Random Forests. *Machine Learning*, 45(1), 5–32

Brown, S., T. Pearson, D. Slaymaker, S. Ambagis, N. Moore, D. Novelo and W. Sabido, 2005. Creating a Virtual Tropical Forest from three-dimensional Aerial Imagery to Estimate Carbon Stocks, *Ecological Applications*, 15(3):1083–1095.

Brown de Colstoun, E.C., M.H. Story, C. Thompson, K. Commisso, T.G. Smith, and J.R. Irons, 2003. National Park vegetation mapping using multitemporal Landsat/data and a decision tree classifier, *Remote Sensing of Environment*, 85(3):316–327.

Budreski, K.A., R. H. Wynne, J. O. Browder, and J. B. Campbell, 2007. Comparison of Segment and Pixel-based Non-parametric Land Cover Classification in the Brazilian Amazon Using Multi-temporal Landsat TM/ETM+ Imagery. *Photogrammetric Engineering and Remote Sensing*,**73**(7): 813.

Cade, B.S., 1997. Comparison of tree basal area and canopy cover in habitat models: Subalpine forest. *J. Wildlife Management*. 61(2), 326–335.

Cao, C., Bao, Y., Xu ,M. , Chen,W., Zhang, H., He,Q. , Li, Z., Guo, H., Li, J., Li X., & Li,G. (2012) Retrieval of forest canopy attributes based on a geometric-optical model using airborne LiDAR and optical remote-sensing data. *International Journal of Remote Sensing* Vol. 33, No. 3, 10 February 2012, 692–709

Case, B.S. and Hall, R.J. 2008. Assessing prediction errors of generalized tree biomass and volume equations for the boreal forest region of West Central Canada. *Canadian Journal of Forest Research*, 38, 878–889

Chastain, R.A., & Townsend, P.A. (2007). Use of landsat ETM and topographic data to characterize evergreen understory communities in appalachian deciduous forests. *Photogrammetric Engineering & Remote Sensing*, 73, 563–575

Chave, J., Andalo, C., Brown, S., Cairns, M., Chambers, J., Eamus, D., Fölster, H., Fromard, F., Higuchi, N., Kira, T., 2005. Tree allometry and improved estimation of carbon stocks and balance in tropical forests. *Oecologia* 145, 87–99.

Chubey, M. S., Franklin, S. E. and Wulder, M. A. (2006). Object-based analysis of Ikonos-2 imagery for extraction of forest inventory parameters. *Photogrammetric Engineering and Remote Sensing* 72(4):383–394.

Clark, M. L., Roberts, D. A., & Clark, D. B. (2005). Hyperspectral discrimination of tropical rain forest tree species at leaf to crown scales. *Remote Sensing of En*vironment, 96, 375−398

Coder, D. K. D. 2000. Crown Shape Factors & Volumes. *Tree Biomechanics Series*. University of Georgia: University of Georgia.

Cohen, W. B., & Spies, T. A. (1992). Estimating structural attributes of Douglas-fir/western hemlock forest stands from Landsat and SPOT imagery. *Remote Sensing of Environment*, 41, 1 – 17.

Cook, S.E., and R.G.V. Bramley, 2000. Coping with variability in agricultural production-Implications for soil testing and fertilizer management. *Communications in Soil Science and Plant Analysis*, 31: 1531–1551.

Commonwealth of Australia, 1999. Comprehensive Regional Assessment, World Heritage Sub-theme: Eucalypt-dominated vegetation. *Report of the Expert Workshop*, Canberra, 8 & 9 March 1999. (Commonwealth of Australia), 105 pages.

Congalton, R.G., 1991. A review of assessing the accuracy of classifications of remotely sensed data. *Remote Sensing of Environment*, **37**(1): 35–46.

Congalton, R.G. and K. Green, 2009. Assessing the accuracy of remotely sensed data: principles and

practices, *CRC/Taylor & Francis, Boca Raton*.

Cutini A, Chianucci F, Manetti MC, 2013. Allometric relationships for volume and biomass for stone pine (*Pinus pinea* L.) in Italian coastal stands. iForest 6: 331–337 [online 2013-08-29] URL: http://www.sisef. it/iforest/contents/?id=ifor0941-006

Dash, J., E. Steinle, R.P. Singh, and H.P. Bähr, 2004. Automatic building extraction from laser scanning data: An input tool for disaster management, *Advances in Space Research*, 33:317–322.

Dare, P. M.. 2005. Shadow Analysis in High-Resolution Satellite Imagery of Urban Areas, *Photogrammetric Engineering & Remote Sensing*, 2005, Vol. 71, No. 2, pp. 169–177.

Dassot, M., Barbacci , A., Colin A., Fournier, M.,and Constant, T. Tree architecture and biomass assessment from terrestrial LiDAR measurements: a case study for some Beech trees (*Fagus sylvatica*). SilviLaser 2010.

Definiens, 2004, eCognition 4 User Guide, *Definiens Imaging GmbH Munich.*

Dehvari A., and Heck R. J., 2009. Comparison of object-based and pixel based infrared airborne image classification methods using DEM thematic layer. *Journal of Geography and Regional Planning*, 2 (4): 086–096.

Drake, J.B.; Dubayah, R.O.; Clark, D.; Knox, R.; Blair, J.B.; Hofton, M.; Chazdon, R.L.; eishampel, J.F.; Prince, S. 2002a. Estimation of tropical forest structural characteristics using large-footprint LIDAR. *Remote Sensing of Environment*. 79: 305–319.

Duveiller, G., P. Defourny, B. Desclee, and, P. Mayaux, 2008. Deforestation in Central Africa: Estimates at regional, national and landscape levels by advanced processing of systematically-distributed Landsat extracts. *Remote Sensing of Environment*, **112**(5): 1969–1981.

Eamus, D., McGuinness, K., and Burrows, W (2000) Review of Allometric Relationships for Estimating Woody Biomass for Queensland, the Northern Territory and Western Australia. National Carbon Accounting System Technical Report No. 5A.

Edson, C., and Wing, M.G. (2011). Airborne Light Detection and Ranging (LiDAR) for individual Tree Stem Location, Height and Biomass Measurements. (2011). *Remote Sensing* (Open Access), doi: 10.3390/rs3112494. Vol. 3, pp 2494–2528

Elliott, H.J., Bashford, R., Greener, A., 1993. Effects of defoliation by the leaf beetle, Chrysophtharta bimaculata, on growth of Eucalyptus regnans plantations in Tasmania. *Aust. Forest*. 56, 22–26.

Fang, D.Q., C.T. Federici, and M.L. Roose. 1998. A high resolution linkage map of the citrus tristeza virus resistance gene region in Poncirus trifoliata (L.) *Raf. Genetics* 150:883–890.

Falcucci, A., L. Maiorano, and L. Boitani, 2007. Changes in land-use/land-cover patterns in Italy and their implications for biodiversity conservation. *Landscape Ecology*, **22**(4): 617–631.

Fisher, P., 1997. The pixel: a snare and a delusion. *International Journal of Remote Sensing*, **18**(3): 679–685.

Flanders, D., M. Hall-Beyer, and J. Pereverzoff, 2003. Preliminary evaluation of eCognition object-based software for cut block delineation and feature extraction. *Canadian Journal of Remote Sensing*, **29**(4): 441–452.

Fleck, S. Mölder, I., Jacob, M., Gebauer, T., Jungkunst, H.F., Leuschner, C., 2011. Comparison of conventional eight-point crown projections with LIDAR-based virtual crown projections in a temperate old-growth forest. *Annals Forest Sci*. 68, 1173–1185.

Foody, G.M., Boyd, D.S., Cutler, M.E.J., 2003. Predictive relations of tropical forest biomass from Landsat TM data and their transferability between regions. *Remote Sensing of Environment* 85, 463-474.
Foody, G.M., 2004. Thematic map comparison: evaluating the statistical significance of differences in classification accuracy. *Photogrammetric Engineering and Remote Sensing*, 70(5): 627–634.

Franklin, J., Strahler, A.H., 1988. Invertible canopy reflectance modeling of vegetation structure in semi-arid woodland. IEEE Trans. *Geoscience and Remote Sensing* 26, 809–825.

François A. Gougeon and Donald G. Leckie. 2006 The Individual Tree Crown Approach Applied to Ikonos Images of a Coniferous Plantation Area. *Photogrammetric Engineering & Remote Sensing* Vol. 72, No. 11, November 2006, pp. 1287–1297.

Fu, K.S. and Mui, J.K. (1981). A survey of image segmentation, *Patter Recognition*, vol 13, pp 3-16

Garraway, E., Lamb, D.W., 2011. Delineating spatial variations in soil carbon using remotely sensed data: A New England case study, *Proceedings of the 2011 Regional Convention, Newcastle Division, Engineers Australia* (R. Patterson Ed.), (Newcastle Division Engineers Australia: Newcastle West, Australia), University of New England, Armidale. NSW 16th -18th September 2011. ISBN 978-0-85825-870-9, 45-52.

García, M., Riaño, D., Chuvieco, E., Danson, F.M., 2010. Estimating biomass carbon stocks for a Mediterranean forest in central Spain using LiDAR height and intensity data. *Remote Sensing of Environment* 114, 816–830.

Gering, L.R., May, D.M., 1995. The Relationship of Diameter at Breast Height and Crown Diameter for Four Species Groups in Hardin County, Tennessee. *Southern J. Appl. Forest*.. 19 (4), 177–181.

Gertner, G.Z**.** 1991. The sensitivity of measurement error in stand volume estimation. In *Canadian Journal of Forest Research*, vol. 20, pp. 800–804.

Gerylo, G., R. J. Hall, S. E. Franklin, A. Roberts, and E. J. Milton, 1998. Hierarchical image classification and extraction of forest species composition and crown closure from airborne multispectral images, *Can. J. Rem. Sen*., 24, (3), 219–232.

Gill, S. J., Biging, G.S., Murphy, E.C., 2000. Modeling conifer tree crown radius and estimating canopy cover. *Forest Ecology and Management* 126, 405–416.

Gitelson, A. A., Kaufmann, Y. J., & Merzlyak, M. N. (1996). Use of Green channel in remote sensing of global vegetation from EOS-MODIS. *Remote Sensing of Environm*ent, 58, 289−298

Goh, K. M., Mansur, I., Mead, D. J., Sweet, G. B., 1996. Biological nitrogen fixing capacity and biomass production of different understorey pastures in a Pinus radiata-pasture agroforestry system in New Zealand. *Agroforest. Sys*. 34, 33–49.

Goodchild, M.F., M. Yuan, and T.J. Cova, 2007. Towards a general theory of geographic representation in GIS. *International Journal of Geographical Information Science*, 21(3): 239– 260.

Goodenough, D. G., Chen, H., Han, D. T., & Li, J. Y. (2005). Multisensor Data fusion for aboveground carbon estimation. *Proceedings of XXVIIIth General Assembly of the International Union of Radio Science* (URSI), October, 23–29, 2005, New Delhi, India (pp. 1−4)

Gougeon, F.A. 1995. A crown-following approach to the automatic delineation of individual tree crowns in high spatial resolution aerial images. *Can. J. Rem. Sensing* 21(3):274–284.

Graham, S., Wilson, B. R., Reid, N. and Jones,H. (2004). Scattered paddock trees, litter chemistry, and surface soil properties in pastures of the New England Tablelands, New South Wales. *Soil Research*, vol. 42, no. 8, pp. 905–912, 2004.

Greenberg, J.A., Dobrowski, S.Z., Ustin, S.L. (2005) "Shadow allometry: Estimating tree structural parameters using hyperspatial image analysis" *Remote Sensing of Environment*, 97:15–25.

Grote, R., 2003. Estimation of crown radii and crown projection area from stem size and tree position. *Annals Forest Sci*. 60, 393–402.

Hall, R.J., Morton, R.T., Nesby, R.N., 1989. A Comparison of Existing Models for DBH Estimation for Large –scale photos. *Forestry Chronicle*. 114–116.

Hall, R., Skakun, R., Arsenault, E., Case, B., 2006. Modeling forest stand structure attributes using Landsat ETM+ data: Application to mapping of aboveground biomass and stand volume. *Forest Ecology and Management* 225, 378–390.

Hamburg, S.P., Zamolodchikov, D.G., Korovin, G.N., Nefedjev, V.V., Utkin, A.I., Gulbe, J.I., Gulbe, T.A., 1997. Estimating the carbon content of Russian forests; a comparison of phytomass/volume and allometric projections. *Mitigation and Adaptation Strategies for Global Change* 2, 247–265.

Haralick, R. and Shapiro, L. (1985). Survey: image segmentation techniques. *Computer Vision, Graphics, and Image Processing*, 29, 100–132.

Haralick, R. M., K. Shanmugam, and I. Dinstein. 1973. Textural features for image classification. *IEEE TransActions on Systems, Man, and Cybernetics* 3:610–21

Haralick, R. M. (1986). Statistical image texture analysis. In T. Y. Young, & K. S. Fu (Eds.), *Handbook of pattern recognition and image processing* (pp. 247–279). New York: New York.

Hardin, P.J., 1994. Parametric and nearest-neighbor methods for hybrid classification: a comparison of pixel assignment accuracy. *Photogrammetric Engineering and Remote Sensing*, 60, 1439– 1448.

Hay, G.J., G. Castilla, M.A.Wulder, J.R. Ruiz, 2005. An automated object-based approach for the multiscale image segmentation of forest scenes. *International Journal of Applied Earth Observation and Geoinformation*, 7: 339–359.

Heikkonen, J., and A. Varfis, 1998. Land-cover land-use classification of urban areas: A remote sensing approach, *International Journal of Pattern Recognition and Artificial Intelligence*, 12(4):475–489.

Heinzel, J.N., Weinacker, H., and Koch, B., 2008. Full automatic detection of tree species based on delineated single tree crowns – a data fusion approach for airborne laser scanning data and aerial photographs, *Proceedings of the SilviLaser 8th international conference on LiDAR applications in forest assessment and inventory*, (pp. 76–85), September 18-19, 2008, Edinburgh, UK.

Hester D.B., S.A.C. Nelson, H.I. Cakir, S. Khorram, and H. Cheshire., 2010. High – resolution landcover change detection based on fuzzy uncertainty analysisand change reasoning. *International Journal of Remote Sensing*, 31(2): 455–475.

Hemery, G.E., Savill, P.S., Pryor, S.N., 2005. Applications of the crown diameter-stem diameter relationship for different species of broadleaved trees. *Forest Ecoogy and Management*.. 215, 285–294.

Hill, R. A., & Thomson, A. G. (2005). Mapping woodland species composition and structure using airborne spectral and LIDAR data. *International Journal of Remote Sensing*, 26, 3763−3779

Hirschmugl, M., Ofner, M., Raggam, J., Schardt, M., 2007. Single tree detection in very high resolution remote sensing data. *Remote Sensing of Environment*, 110, pp. 533–544.

Houghton, R.A., 2005. Aboveground forest biomass and the global carbon balance. *Global Change Biol*. 11, 945–958.

Hollaus, M., Wagner, W., Schadauer, K., Maier, B., Gabler, K., 2009. Growing stock estimation for alpine forests in Austria: a robust lidar-based approach. *Canadian Journal of Forest Research* 39(7), 1387−1400.

Holmgren, J., & Persson, A. (2004). Identifying species of individual trees using airborne laser scanner. *Remote Sensing of Environ*ment, 90, 415−423

Huertas, A., and Nevatia, R. (1988). "Detecting Buildings in Aerial Images," *Computer Vision, Graphics and Image Processing*, 41(2):131–152.

Hudak, A.T., Crookston, N.L., Evans, J.S., Falkowski, M.J., Smith, A.M.S., Gessler, P.E., Morgan, P., 2006. Regression modeling and mapping of coniferous forest basal area and tree density from discrete-return lidar and multispectral satellite data. *Canadian Journal of Remote Sensing* 32, 126–138.

Hudak, A.T.; Evans, J.S.; Stuart Smith, A.M. LiDAR Utility for Natural Resource Managers. *Remote Sening.* **2009**, *1*, 934–951

Hunter, M.O., Keller, M., Victoria, D. and Morton, D.C. (2013). Tree height and tropical forest biomass estimation. *Biogeosciences*, 10: 8385–8399

Huiyan,G.U., Limin, D., Gang, W., Dong, X., Shunzhong, W & Hui, W. Estimation of forest volumes by integrating Landsat TM imagery and forest inventory data *Science in China*: *Series E Technological Sciences* 2006 Vol.49 Supp. I 54—62 DOI: 10.1007/s11431-006-8107-z

Hyyppa, J., Hyyppa, H., Leckie, D., Gougeon, F., Yu, X., and Maltamo, M. (2008) Review of methods of small footprint airborne laser scanning for extracting forest inventory data in boreal forests. *International Journal of remote Sensing*, 29(5), 1339–1366.

Im, J., Jensen, J. R., & Hodgson, M. E. (2008). Object-based land cover classification using high-posting-density LIDAR data. *GIScience & Remote Sensing*, 45, 209−228.

Irving, R., and McKeown, D. (1989). "Methods for exploiting the Relationship Between Buildings and their Shadows in Aerial Imagery," *IEEE Transactions on Systems, Man and Cybernetics, SMC* 19(6): 1564–1575.

Jensen, J.R., 2009. Remote sensing of the environment, *Pearson Education India*.

Jennings, S.B., Brown, N.D., Sheil, D., 1999. Assessing forest Canopies and Understorey illumination: canopy closure, canopy cover and other measures. *Forestry*. 72 (1), 59–73.

Jobin, B., S. Labrecque, M. Grenier, and G. Falardeau, 2008. Object-based classification as an alternative approach to the traditional pixel-based classification to identify potential habitat of the Grasshopper Sparrow. *Environmental Management*, 41(1): 20–31.

Jonson, J. H., and Freudenberger, D. 2011. Restore and sequester: estimating biomass in native Australian woodland ecosystems for their carbon-funded restoration. CSIRO PUBLISHING

Australian Journal of Botany, 59, 640–653 http://dx.doi.org/10.1071/BT11018

Johansen, K., N. C. Coops, S.E. Gergel, and Y. Stange, 2007. Application of high spatial resolution satellite imagery for riparian and forest ecosystem classification. *Remote Sensing of Environment*, 110(1): 29–44.

Kamagata N., Hara K., Mori M., Akamatsu Y., Li Y., Hoshino Y. (2006) - A new method of vegetation mapping by object-based classification using high resolution satellite data. In: First *International Conference on Object-based Image Analysis* (OBIA 2006), XXXVI (4/C42) Salzburg, Austria.

Ke, Y., Quackenbush, L.J.L., 2011. A review of methods for automatic individual tree-crown detection and delineation from passive remote sensing. *International Journal of Remote Sensing* 32, 4725–4747.

Ke, Y. and L.J. Quackenbush, 2008. Comparison of individual tree crown detection and delineation methods, *In Proceedings of 2008 ASPRS Annual Conference* (American Society of Photogrammetry and Remote Sensing, Bethesda, Maryland), April 28-May 2, 2008, Portland, Oregon.

Ke, Y., Quackenbush, L.J.L., and Im. J.,2010. Synergistic use of Quickbird imagery and lIDAr data for object based forest species classification. *Remote Sensing of Environment*.114, 1141–1154.

Keith, H., Barrett, D., and Keenan, R (2000) Review of Allometric Relationships for Estimating Woody Biomass for New South Wales, The Australian Capital Territory, Victoria, Tasmania and South Australia. National Carbon Accounting System Technical report No. 5B

Kini, A.U., and Popescu, S.C. (2004). TreeVaW : A versatile tool for Analysing Forest Canopy LiDAR Data – A Preview with an Eye towards Future. *In Proceedings of the ASPRS 2004 Fall Conference, Kansas City, MO, USA*, 12–16 September 2004; pp1–10

Kim HY, Lieffering M, Kobayashi K, Okada M, Miura S. 2003. Seasonal changes in the effects of elevated CO2 on rice at three levels of nitrogen supply: a free air CO2 enrichment (FACE) experiment. *Global Change Biology* 9: 826–837.

Kim M., Madden M. (2006) - Determination of optimal scale parameter for alliance-level forest classification of multispectral IKONOS image. Commission IV, WG IV/4 on *Proceeding of 1st OBIA Conference*, 4-5 July, Salzburg, Austria.

Kim S., 2010. LiDAR based species classification using multivariate cluster analysis. *ASPRS Annual Conference*. San Diego, California, April 26-30.

Köstner, B., Falge, E., Tenhunen, J. D., 2002. Age-related effects on leaf area/sapwood area relationships, canopy transpiration and carbon gain of Norway spruce stands (Picea abies) in the Fichtelgebirge, Germany. *Tree Physiol*.. 22, 567–574.

Krosgad, F., and Schiess, P. 2004 – The Allure and pitfalls of using LIDAR topography in harvest and road design. *Proceedings of 12th International Mountain Logging Conference. June 13-16, 2004, Vancouver, B.C.*

Kuyah, S., Dietz, J., Muthuri, C., Jamnadass, R., Mwangi, P., Coe, R., Neufeldt, H., 2012. Allometric equations for estimating biomass in agricultural landscapes: I. Aboveground biomass. *Ag. Ecosys. Enviro.* 158, 216–224.

Landsberg, J., Ohmart, C., 1989. Levels of insect defoliation in forests: patterns and concepts. Trends *Res. Ecol. Evol*.. 4, 96–100.

Lamb, D.W., 2000. The use of qualitative airborne multispectral imaging for managing agricultural crops – A case study in south eastern Australia. *Australian Journal of Experimental Agriculture*, 40(5): 725–738.

Lamb, D.W., M. Trotter, A. Murphy, and I. Young, 2013. "UNE SMART Farm: Showcasing the value of broadband connectivity in the business snd lifestyle of farming". In. *Proceedings of the Digital Rural Futures Conference*. D.W.Lamb (Editor), 26-28th June 2013 (University of New England: Australia), 89.

Lambert, M., Ung, C., Raulier, F., 2005. Canadian national tree aboveground biomass equations. *Canadian Journal of Forest Research* 35, 1996–2018.

Lara A. Arroyo, , Kasper Johansen , John Armston , Stuart Phinn Integration of LiDAR and QuickBird imagery for mapping riparian biophysical parameters and land cover types in Australian tropical savannas. *Forest Ecology and Management* 259 (2010) 598–606

Laymon, 2005. Landcover classification comparison with different resolution imagery. *http://www.ncrste.msstate.edu.* Accessed May 2012.

Leblon B., Gallant L. and Granberg H. (1996). Effects of shadowing types on ground-measured visible and near-infrared shadow reflectances. *Remote Sensing of Environment*. 58(3): 322–328.

Leckie, D.G., Gougeon, F., Walsworth, N., and Paradine, D. (2003). Stand delineation and composition estimation using semi automated individual tree+ crown analysis. *Remote Sensing of Environment*, 85, 355–369

Leckie, D., Gougeon, F., Hill, D., Quinn, R., Armstrong, L., & Shreenan, R. (2003). Combined high density LiDAR and multispectral imagery for individual tree crown analysis. *Canadian Journal of Remote Sensing*, 29, 633−649

Leckie, D.G., and Gillis, M.D., "Forest inventory in Canada with emphasis on map production". The *Forestry Chronicle*., vol. 71, no. 1, pp. 74–88, 1995

Lee, A.C., Lucas, R.M., 2007. A Lidar-derived canopy density model for tree stem and crownmapping in Australian forests. *Rem. Sens. Env*. 111(4), 493–518.

Lefsky, M.A., Cohen, W.B., Parker, G.G., and Harding, D.J., 2002a. Lidar remote sensing for ecosystem studies, *Bioscience*, Vol. 52, No. 1, pp.19–30.

Lefsky, M.A., Cohen, W.B., Harding, D.J., Parker, G.G., Acker, S.A., and Gower, S.T., 2002b. Lidar remote sensing of above-ground biomass in three biomes, *Global Ecology & Biogeography*, No. 11, pp. 393–399.

Lefsky, M.A., Harding, D., Cohen, W.B., Parker, G., and Shugart, H.H., 1999a. Surface lidar remote sensing of basal area and biomass in deciduous rorests of Eastern Maryland, USA, Remote Sensing of Environment, No. 67, pp. 83–98. *ASPRS 2008 Annual Conference Portland, Oregon* ♦ April 28 – May 2, 2008

Lefsky, M.A., Cohen, W.B., Acker, S.A., Parker, G.G., Spies, T.A., and Harding, D., 1999b. Lidar remote sensing of the canopy structure and biophysical properties of Douglas-fir western hemlock forests, *Remote Sensing of Environment*, (70) pp. 339–361.

Leverett, R. (2010). Measuring Tree Height by Tape and Clinometer Scenarios. *Bulletin of the Eastern Native Tree Society*, 5(3-4): 3–12.

Liang, X., Hyyppa, J., & Matikainen, L. (2007). First-last pulse signatures of airborne laser

scanning for tree species classification, Deciduous–coniferous tree classification using difference between first and last pulse laser signatures. *Proceedings of the ISPRS workshop, Laser Scanning 2007 and Silvilaser 2007* (pp. 253−257).

Lim, K., Hopkinson, C., and Treitz, P.(2008) Examining the effects of sampling point densities on laser canopy height and density metrics. *Forestry Cronicle*, 84(6), pp. 876–885

Lim, K.S., Treitz, P.M., 2004. Estimation of above ground forest biomass from airborne discrete return laser scanner data using canopy-based quantile estimators. *Scandinavian Journal of Forest Research* 19, 558–570.

Lindeberg ,T. "Feature detection with automatic scale selection", *International Journal of Computer Vision*, vol. 30, no. 2, pp. 77–116, 1998

Liow, Y., and T. Pavlidis, T. (1990). "Use of Shadows for Extracting Buildings in Aerial Images," *Computer Vision, Graphics and Image Processing*, 49: 242-277 Liu W., Yamazaki F., 2012. Object-based shadow

Liu, H., D. Sherman, and S. Gu, 2007. Automated extraction of shorelines from airborne light detection and ranging data and accuracy assessment based on Monte Carlo simulation, *Journal of Coastal Research*, 23:1359–1369.

Liu, X., Zhang, Z., Peterson, J. and Chandra, S. 2007. LiDAR-derived high quality ground control information and DEM for image orthorectification. *GeoInformatica* 11(1), 37–53.

Loos, R., Niemann, O., 2006. Identification of individual trees and canopy shapes using LiDAR data for fire management. *IEEE*, pp. 3755–3757.

Loos, R., Niemann, O., Visintini, F., 2007. Identification of partial canopies using first and last return lidar data. *Our Common Borders – Safety, Security, and the Environment Through Remote Sensing* October 28 – November 1, 2007, * Ottawa, Ontario, Canada

Lu, D. and Weng, Q. 2007. A survey of image classification methods and techniques for improving classification performance, *International Journal of Remote Sensing*, 28:5, 823-870.

Lu, D., 2006. The potential and challenge of remote sensing-based biomass estimation. *International Journal of Remote Sensing* 27, 1297–1328.

Machala, M. and Zejdová, L.2014. Forest Mapping Through Object-based Image Analysis of Multispectral and LiDAR Aerial Data. *European Journal of Remote Sensing* - 2014, 47: 117–131 doi: 10.5721/EuJRS20144708

Maclean, G.A., and Krabill, W. B. (1986), Gross merchantable timber volum estimation using airborne Lidar system, *Canadian Journal of Remote Sensing*, Vol. 12, pp 7–18

Makungwa, S.D., Chittock, A., Skole, D.L., Kanyama-Phiri, G.Y., Woodhouse, I.H., 2013. Allometry for Biomass Estimation in Jatropha Trees Planted as Boundary Hedge in Farmers' Fields. *Forests*. 4, 218–233.

Malimbwi, R., Solberg, B., Luoga, E., 1994. Estimation of biomass and volume in miombo woodland at Kitulangalo Forest Reserve, Tanzania. *Journal of Tropical Forest Science* 7, 230-242.

Maltamoa, M., , Eerika¨inenb, K., Pitka¨nena, J., Hyyppa¨ J., and Vehmasa., M. (2004) Estimation of timber volume and stem density based on scanning laser altimetry and expected tree size distribution functions. *Remote Sensing of Environment* 90 (2004) 319 – 330

Manakos, I., T. Schneider, U. Ammer, 2000. *A comparison between the ISODATA and the eCognition classification methods on basis of field data*. *IAPRS* 33, 133–139.

Manning, A.D., Fischer, J. and Lidenmayer, D.B. 2006. Scattered trees are keystone structures. Implications for conservation. *Biological. Conservation.* 132, 311–321

Mathieu R., Aryal,J. and Chong A. K., , "Object-Based Classification of IKONOS Imagery for Mapping Large-Scale Vegetation Communities in Urban Areas", *Sensors*, vol.7, pp. 2860–2880, 2007

McComb, J. W., Roberts, S. D., & Evans, D. L. (2003). Influence of fusing lidar and multispectral imagery on remotely sensed estimates of stand density and mean tree height in a managed loblolly pine plantation. *Forest Science*, 49, 457 – 466.

Mcinerney, D.O., Suarez-Minguez, J., Valbuena, R., and Nieuwenhuis, 649 M., 2010, Forest canopy height retrieval using Lidar data, medium-resolution 650 satellite imagery and kNN estimation in Aberfoyle, Scotland. *Forestry*, 83, pp. 651 195−206.

McGaughey, R. (2010). FUSION/LDV: Software for LIDAR Data Analysis and Visualization. United States Department of Agriculture Forest Service Pacific Northwest Research Station FUSION/LDV: Version 2.90

Medhurst, J.L. and Beadle, C.L. (2001) Crown structure and leaf area index development in thinned and unthinned Eucalyptus nitens plantations. *Tree Physiology*, 21: 989–999.

Minho, K., 2009. Object-based spatial classification of forest vegetation with ikonos imagery, *Ph.D. Dissertation, University of Georgia, Georgia*, 133p.

Moeur, M., 1997. Spatial models of competition and gap dynamics in old growth Tsuga heterophylla/Thuja plicata forests. *Forest Ecol. Man*. 94, 175–186.

Mundt, J.T., N.F. Glenn, K.T. Weber, and J. Pettingill, 2006. Determining target detection limits and accuracy delineation using an incremental technique. *Remote Sensing of Environment*, 105, 34– 40.

Myint S.W., Gober P., Brazel A., Grossman-Clarke S., Weng Q. (2011) - Per-pixel vs. object-based classification of urban land cover extraction using high spatial resolution imagery. *Remote Sensing of Environment*, 115 (5): 1145–1161. doi: http://dx.doi. org/10.1016/j.rse.2010.12.017

Næsset, E., & Bjerknes, K.-O. 2001. Estimating tree heights and number of stems in young forest stands using airborne laser scanner data. *Remote Sensing of Environment*, 78, 328–340

National Parks and Wildlife Service, 2003. Duval Nature Reserve, Plan of Management. (*Commonwealth of Australia*) ISBN 0 7313 6600 X, 17 pages.

Næsset, E., Økland, T., 2002. Estimating tree height and tree crown properties using airbo rne scanning laser in a boreal nature reserve. *Remote Sensing of Environment* 79, 105–115.

Nelson, R., Krabill, W. and Maclean, G. 1984: Determining forest canopy characteristics using airborne laser data. *Remote Sensing of Environment* 15, 201–12.

Nelson, R., Krabill, W. & Tonelli, J. 1988a. Estimating forest biomass and volume using airborne laser data. *Remote Sens. Environ*. 24: 247–267.

Nelson R., 1997. Modelling forest canopy heights. The effects of canopy shape. *Rem. Sens. Env*. 60, 327–334.

Neumann, F.G., 1993. Insect pest problems of eucalypt plantations in Australia. 3. Victoria. *Australian Forest.* 56, 370–374.

O'Brien, S.T., Hubbell, S.B.Spiro, P., Condit, R., Foster, R.B., 1995. Diameter, height, crown and age relationships in eight neotropical tree species. *Ecology.* 76 (6), 1926–1939.

Oliver, I., Pearce, S., Greenslade, P. J. M., Britton, D. R., 2006. Contribution of paddock trees to the conservation of terrestrial invertebrate biodiversity within grazed native pastures. *Australian Ecol*. 31, 1–12.

Orka, H.O., Nasset, E and Bollandsas, O.M. 2007. Utilizing airborne laser intensity for tree speciesclassification. Onternational Archives of the *Photogrammetry, remote Sensing and Spatial Information Sciences* 36. Part3/W52:300–304

Ozdemir , I. (2008) Estimating stem volume by tree crown area and tree shadow area extracted from pan-sharpened Quickbird imagery in open Crimean juniper forests. *International Journal of Remote Sensing*. Vol 29. Pages 5643–5655

Palace, M., M. Keller, G. P. Asner, J. N. M. Silva, and C. Passos. 2007. Necromass in undisturbed and logged forests in the Brazilian Amazon. *Forest Ecology and Management* 238: 309–318.

Paul, K. I., Roxburg, S. H., Ritson , P., Brooksbank, K., England, J. R., Larmour, J. S., Raison, J.R., Peck, A., Wildy, D. T., Sudmeyer, R. A., Giles, R., Carter, J., Bennett, R., Mendham, D. S., Huxtable, D., and Bartle, J. R. 2013. *Forest Ecology and Management* 310, 1005–1015

Persson, A., Holmgren, J. and Soderman, U. 2002. Detecting and measuring individual trees using and airborne alser scanner. *Photogrammetric Engineering and remote Sensing* 68:925–932

Phua, M.H., Saito, H., 2003. Estimation of biomass of a mountainous tropical forest using Landsat TM data. *Canadian Journal of Remote Sensing* 29, 429-440.

Platt, R.V., and L. Rapoza, 2008. An evaluation of an Object-Oriented Paradigm for Land Use/Land Cover Classification. *The Professional Geographer*, 60(1): 87–100.

Popescu, S.C., Wynne, R.H., 2004a. Seeing the trees in the forest: using lidar and multispectral data fusion with local filtering and variable window size for estimating tree height. *PERS.* 70 (5), 589–604.

Popescu, S.C., Wynne, R.H., Scrivani, J.A., 2004b. Fusion of small-footprint Lidar and multispectral data to estimate plot-level volume and biomass in deciduous and pine forests in Virginia, USA. *Forest Sci.* 50 (4), 551–564.

Popescu, S.C., et al (2002). Estimating plot level tree heights with LiDAR: local filtering with a canopy height based variable window size. *Computers and Electronics in Agriculture.* 37(103),pp. 71–95.

Popescu, S.C., Wynne, R.H., and Nelson, R.F. (2003) Measuring individual tree crown diameter with LiDAR and assessing its influence on estimating forest volume and biomass. *Canadian journal of Remote Sensing*, Vol. 29, No. 5, pp. 564–577

Popescu, S. C. (2007). Estimating biomass of individual pine trees using airborne lidar. *Biomass & Bioenergy*, 31, 646–655.

Pouliot, D.A., D.J. King, F.W. Bell, and D.G. Pitt, 2002. Automated tree crown detection and delineation in high-resolution digital camera imagery of coniferous forest regeneration, *Remote Sensing of Environment*, 82:322–334

Pretzsch, H., 2009. Forest dynamics, growth and yield: From measurement to model. *Springer*. 664 pages.

Puissant, A., J. Hirsch, and C. Weber, 2005. The utility of texture analysis to improve per-pixel classification for high to very high spatial resolution imagery. *International Journal of Remote Sensing*, **26**(4): 733–745.

Ravindranath, N.H., Ostwald, M., 2008. Carbon inventory methods: handbook for greenhouse gas inventory, carbon mitigation and roundwood production projects. *Springer Verlag*.

Reitberger, J., Krzystek, P., Stilla, U. 2006. Analysis of fill waveform LIDAR data for tree species classification. *Symposium of ISPRS commission III Photogrammetric Computer Vision PCV'06*. Bonn, Germany. 20-22 September 2006. IAPRS, XXXVI, Part 3: 228–233

Robertson, L.D. and D.J. King, 2011. Comparison of pixel-and object-based classification in land cover change mapping. *International Journal of Remote Sensing*, 32(6): 1505–1529.

Röhle H., Huber W., 1985. Untersuchungen zur Methode der Ablotung von Kronenradien und der Berechnung von Kronengrundflächen, *Forstarchiv*. 56, 238–243.

Roy, P., Ravan, S.A., 1996. Biomass estimation using satellite remote sensing data—an investigation on possible approaches for natural forest. *Journal of Biosciences* 21, 535-561.

Ryherd, S., C. Woodcock, 1996. Combining spectral and texture data in the segmentation of remotely sensed images. *Photogrammetric Engineering and Remote Sensing*, 62, 181–194.

Sanquetta, C.R., Dalla Corte, A.P., Silva. F.S., 2011a. Biomass expansion factor and root-to-shoot ratio for Pinus in Brazil. *Carbon Bal. Man*. 6(6), 1–8.

Sanquetta, C.R., Dalla Corte, A.P., Jacon. A.D., 2011b. Crown area and trunk diameter relationship for tree species at a mixed-araucaria natural forest in the mid-southern Parana State, Brazil. *Floresta*. 41 (1), 63–72.

Scurlock, J., Johnson, K., Olson, R., 2002. Estimating net primary productivity from grassland biomass dynamics measurements. *Global Change Biology* 8, 736–753.

Shackelford, A.K., and C.H. Davis, 2003. A combined fuzzy pixel-based and object-based approach for classification of high-resolution multispectral data over urban areas. *IEEE Transactions on Geoscience and Remote Sensing*, 41(10): 2354–2363.

Shahtahmassebi, A., Yang N., Wang K., Moore, N. and Shen Z. (2013). Review of shadow detection and de-shadowing methods in remote sensing. *Chinese Geographical Science*, 23(4): 403–420.

Shettigara, V.K., and Sumerling, G.M. (1998) Height determination of extended objects using shadows in SPOT images. *Photogrammetric Engineering and Remote Sensing*, 64 (1): 35–44.

Smith, M.W., 2008. Relationship of trunk size to selected canopy size parameters for native pecan trees. *HortSci*. 43(3), 784–786.

Smith, J.L. and J. J. Halvorson. 2011. Field Scale Studies on the spatial Variability of soil quality indicators in Washington State, USA. *Applied and Environmental Soil science*, Volume 2011, Article ID 198737, 7 pages, doi:10.1155/2011/198737(2011).

Snowdon, P., Raison, J., Keith, Heather., Ritson, P., Grierson, P., Adams, M., Montagu, K., Bi, Hui-quan., Burrows, W., Eamus, D., 2002. Protocol for Sampling Tree and Stand Biomass. National Carbon Accounting System, *Technical Report No. 31* (Australian Greenhouse Office).

Sobrino, J., and N. Raissouni, 2000. Toward remote sensing methods for land cover dynamic monitoring: application to Morocco. *International Journal of Remote Sensing*, 21(2): 353–366.

Soto-Pinto, L., Anzueto, M., Mendoza, J., Ferrer, G.J., de Jong, B., 2010. Carbon sequestration through agroforestry in indigenous communities of Chiapas, Mexico. *Agroforest Sys*. 78, 39–51.

Song, C., Dickinson, M. B., Su, L., Zhang, S., and Yaussey, D. 2010. Estimating average tree crown size using spatial information from Ikonos and QuickBird images: Across-sensor and across-site comparisons. *Remote Sensing of Environment* 114 (2010) 1099–1107

Steininger, M., 2000. Satellite estimation of tropical secondary forest above-ground biomass: data from Brazil and Bolivia. *International Journal of Remote Sensing* 21, 1139-1157.

Stromgaard, P., 1985. Biomass estimation equations for miombo woodland, Zambia. *Agroforestry systems* 3, 3-13.

Sumida, A., Komiyama, A. 1997. Crown spread patterns for five deciduous broad-leaved woody species: Ecological significance of the retention patterns of larger branches. *Annals of Biol*. 80, 759–766.

Tadesse, W., Coleman, T.L. and T.D. Tsegaye (2003). Improvement of Landuse and Land-cover Classification of an Urban Area Using Image Segmentation from Landsat ETM+ Data. Proceedings of the 30th *International Symposium on Remote Sensing Environment*, November 10-14, 2003, Honolulu, Hawaii.

Ter-Mikaelian, M.T., Korzukhin, M.D., 1997. Biomass equations for sixty-five North American tree species. *Forest Ecol. Man*. 97, 1–24.

Thenkabail, P.S., Stucky, N., Griscom, B.W., Ashton, M.S., Diels, J., Van Der Meer, B., Enclona, E., 2004. Biomass estimations and carbon stock calculations in the oil palm plantations of African derived savannas using IKONOS data. *International Journal of Remote Sensing* 25, 5447-5472.

Thomas, N., C. Hendrix, and R.G. Congalton, 2003. *A* comparison of urban mapping methods using high-resolution digital imagery. *Photogrammetric Engineering and Remote Sensing*, 69(9): 963– 972.

Tonolli, S., Dalponte, M., Vescovo, L., Rodeghiero, M., Bruzzone, L., Gianelle, D., 2011. Mapping and modeling forest tree volume using forest inventory and airborne laser scanning. *European Journal of Forest Research*, 1–9.

Todd, K.W., Csillag, F., and Atkinson, P.M., 2003. Three-dimensional mapping of light transmittance and foliage distribution using lidar, *Canadian Journal of Remote Sensing*, Vol. 29, No. 5, pp. 544–555.

Townshend J.R.G., Huang C., Kalluri S.N.V., Defries R.S., Liang S., Yang K. (2000) . Beware of Per-pixel Characterization of Land Cover. *International Journal of Remote Sensing*, 2000, vol. 21, no. 4, 839–843

Tumbo, S. D., Salyani, M., Whitney, J. D., Wheaton ,T. A., Miller ,W. M. 2002. Investigation of laser and ultrasonic ranging sensors for measurements of citrus canopy volume. *Applied Engineering in Agriculture* Vol. 18(3): 367–372

Unger,D.R., Hung, I-Kuai, Brooks, R. & Williams, H. *GIScience & Remote Sensing* Volume 51, Issue 3, 2014.

van Ewijk, K. Y., Randin, C.F., Treitz, P.M., and Scott, N. A. 2014. Predicting fine-scale tree species abundance patterns using biotic variables derived from LiDAR and high spatial resolution imagery. *Remote Sensing of Environment* 150 (2014) 120–131

Verma, N.K., Lamb, D.W, Reid, N. and Wilson, B. (2014a) "An allometric model for estimating DBH of isolated and clustered Eucalyptus trees from measurements of crown projection area", *Forest Ecology and Management*. 326: 125–132.

Verma, N.K., Lamb, D.W., Reid, N. and Wilson, B. (2013) "Tree cover extraction from 50 cm worldview imagery: A comparison of image processing techniques". *IEEE International Geoscience & Remote Sensing Symposium, IGARSS* 2013, July 21-26, 2013, Melbourne, Australia. 192–195.

Verma, N., Lamb, D.W., Reid, N. and Wilson, B. (2014b) "A comparative study of land cover classification techniques for 'farmscapes' using very high-resolution remotely sensed data", *Photogrammetric Engineering and Remote Sensing.* 80 (5), 461–470

Vieira ICG, de Almeida AS, Davidson EA, Stone TA, de Carvalho CJR, Guerrero JB. Classifying successional forests using Landsat spectral properties and ecological characteristics in eastern Amazonia.*Remote Sensing of Environment*. 2003;87:470–481.

Wang, L., W. Sousa, and P. Gong, 2004. Integration of object-based and pixel-based classification for mapping mangroves with IKONOS imagery. *International Journal of Remote Sensing*, 25(24): 5655–5668.

Wang, L., Gong, Peng, Biging, G.S.G., 2004. Individual tree-crown delineation and treetop detection in high-spatial-resolution aerial imagery. *Photogrammetric Engineering and Remote* 3114, 351–358.

Walraven, R. (1978). Calculating the Position of the Sun. *Solar Energy*, 30: 393–397.

Weber, K.T., J. Théau, K. Serr, 2008. Effect of coregistration error on patchy target detection using high-resolution imagery. *Remote Sensing of Environment*, 112, 845–850.

West, G. and Glasby, T. (2010). A new system for high resolution mapping of seagrass. Proc 19th *NSW Coastal Conference* ("Coastal Management – all aboard, making it work!"), 10 – 12 November 2010, Batemans Bay, NSW, Australia.

Wheaton, T. A., J. D. Whitney, W. S. Castle, R. P. Muraro, H. W. Browning, and D. P. H. Tucker.1995. Citrus scion and rootstock, topping height, and tree spacing affect tree size, yield, fruit quality and economic return. *J. Amer. Soc. Hort. Sci.* 120(5): 861–870

White, J., 1981. The allometric interpretation of the self-thinning rule. *J. Theoret. Biol*. 89, 475–500.

Wilson, B. R., Growns,I. and Lemon, J., "Scattered native trees and soil patterns in grazing land on the Northern Tablelands of New South Wales, Australia", *Soil Research*, vol. 45, no. 3, pp. 199–205

Williams, R.J., Zerihun, A., Montagu, K.D., Hoffman, M., Hutley, L.B., and Chen, X. 2005. Allometry for estimating aboveground tree biomass in tropical and subtropical eucalypt woodlands. *Australian Journal of Botany*, 53, 607–619

Willhauck, G., 2000. Comparison of object oriented classification techniques and standard image analysis for the use of change detection between SPOT multispectral satellite images and aerial photos. *International Archives of Photogrammetry and Remote Sensing*. Vol. XXXIII, Part B3. Amsterdam.

Wilson, B. R., 2002. Influence of scattered paddock trees on surface soil properties: a case study of the Northern Tablelands of NSW. *Ecol. Man. Restor.* 3, 211–219.

Wong, T.h., Mansor, S.B., Mispan, M.R., Ahmad, N. and W.N.A. Sulaiman (2003). Feature extraction based on object oriented analysis. *Proceedings of ATC 2003 Conference*, 20-21 May 2003, Malaysia.

Woodcock, C.E. and Strahler, A.H. 1987. The factor of scale in Remote sensing. *Remote Sensing of Environment*, 21, 311–332

Wulder, M. A., & Seemann, D. (2003). Forest inventory height update through the integration of lidar data with segmented Landsat imagery. *Canadian Journal of Remote Sensing*, 29, 536−543.

Wulder, M.A., Hall, R.J., Coops, N.C., Franklin, S.E., 2004. High spatial resolution remotely sensed data for ecosystem characterization. *Bioscience* 54, 511–521

Xiuwan, C., 2002. Using remote sensing and GIS to analyse land cover change and its impacts on regional sustainable development. *International Journal of Remote Sensing*, 23(1): 107–124.

Yan, G., J.F. Mas, B.H.P. Maathuis, Z. Xiangmin, and P. M. Van Dijk, 2006. Comparison of pixel-based and object-oriented image classification approaches—a case study in a coal fire area, Wuda, Inner Mongolia, China. *International Journal of Remote Sensing*, 27(18): 4039–4055.

Yemefack, M., D.G. Rossiter, R. Njomgang, *2005.* Multiscale characterization of soilvariability within an agricultural landscape mosaic system in southern Cameroon. *Geoderma*, Volume 125, Issue 1-2: 117–143.

Yinghai Ke, Lindi J. Quackenbush □, Jungho Im. Synergistic use of QuickBird multispectral imagery and LIDAR data for object-based forest species classification. *Remote Sensing of Environment* 114 (2010) 1141–1154

Yu, Q., P. Gong, N. Clinton, G. Biging, M. Kelly, and D. Schirokauer, 2006. Object-based detailed vegetation classification with airborne high spatial resolution remote sensing imagery. *Photogrammetric Engineering and Remote Sensing*, 72(7): 799–811.

Zhang Q. and J. Wang (2003). A rule-based urban landuse inferring method for fine-resolution multispectral imagery. *Canadian Journal of Remote Sensing*, Col. 29, No. 1 pp. 1–13.

Zheng, D., Rademacher, J., Chen, J., Crow, T., Bresee, M., Le Moine, J., Ryu, S.R., 2004. Estimating aboveground biomass using Landsat 7 ETM+ data across a managed landscape in northern Wisconsin, USA. *Remote Sensing of Environment* 93, 402-411.